
Learn2Mix: Training Neural Networks Using Adaptive Data Integration

Shyam Venkatasubramanian¹

Vahid Tarokh¹

¹Duke University, Durham, North Carolina, USA

Abstract

Accelerating model convergence within resource-constrained environments is critical to ensure fast and efficient neural network training. This work presents *learn2mix*, a novel training strategy that adaptively adjusts class proportions within batches, focusing on classes with higher error rates. Unlike classical training methods that use static class proportions, *learn2mix* continually adapts class proportions during training, leading to faster convergence. Empirical evaluations conducted on benchmark datasets show that neural networks trained with *learn2mix* converge faster than those trained with existing approaches, achieving improved results for classification, regression, and reconstruction tasks under limited training resources and with imbalanced classes. Our empirical findings are supported by theoretical analysis.

1 INTRODUCTION

Deep neural networks have become essential tools across various applications of machine learning, including computer vision [Krizhevsky et al., 2012, Simonyan and Zisserman, 2014, He et al., 2016], natural language processing [Vaswani et al., 2017, Devlin et al., 2018, Radford et al., 2019, Touvron et al., 2023], and speech recognition [Hinton et al., 2012, Baeveski et al., 2020]. Despite their ability to learn and model complex, nonlinear relationships, deep neural networks often require substantial computational resources during training. In resource-constrained environments, this demand poses a significant challenge [Goyal et al., 2017], making the development of efficient and scalable training methodologies increasingly crucial to fully leverage the capabilities of deep neural networks.

Training deep neural networks relies on the notion of empirical risk minimization [Vapnik and Bottou, 1993], and typically involves optimizing a loss function using gradient-based algorithms [Rumelhart et al., 1986, Bottou, 2010, Kingma and Ba, 2014]. Techniques such as regularization

[Srivastava et al., 2014, Ioffe and Szegedy, 2015] and data augmentation [Shorten and Khoshgoftaar, 2019], learning rate scheduling, [Smith, 2017] and early stopping [Prechelt, 1998], are commonly employed to enhance generalization and prevent overfitting. However, the efficiency of the training process itself remains a critical concern, particularly in terms of convergence speed and computational resources.

Within this context, adaptive training strategies, which target enhanced generalization by modifying aspects of the training process, have emerged as promising approaches. Methods such as curriculum learning [Bengio et al., 2009, Graves et al., 2017, Wang et al., 2021] adjust the order and difficulty of training samples to facilitate more effective learning. Insights from these adaptive training strategies can be extended to the class imbalance problem [Wang et al., 2019], where underrepresented classes are intrinsically harder to learn due to data scarcity [Buda et al., 2018], a challenge intensified in adversarial settings where safe data collection is severely limited [Wang and Gursoy, 2023]. These methods are typically categorized into data-level methods, such as oversampling and undersampling [Chawla et al., 2002], and algorithm-level approaches, including class-balanced loss functions [Lin et al., 2017]. However, developing adaptive neural network training methodologies that *accelerate* model convergence, while ensuring robustness to class imbalance, remains an open problem.

Building upon these insights, a critical aspect of training efficiency lies in the composition of batches used during stochastic gradient descent. Classical training paradigms maintain approximately fixed class proportions within each shuffled batch, mirroring the overall class distribution in the training dataset [Buda et al., 2018, Peng et al., 2019]. However, this static approach fails to account for the varying levels of difficulty associated with different classes, which can hinder optimal convergence rates. For example, classes with higher error rates or those that are inherently more challenging may require greater emphasis during training to enhance model performance. Ignoring these nuances can lead to suboptimal learning trajectories and prolonged training periods. While existing approaches address class imbalance by adjusting sample weights or dataset resampling, they do not dynamically change the class-wise composition of batches during training via real-time performance metrics.

GitHub repository: <https://tinyurl.com/yy7tfsp5>.

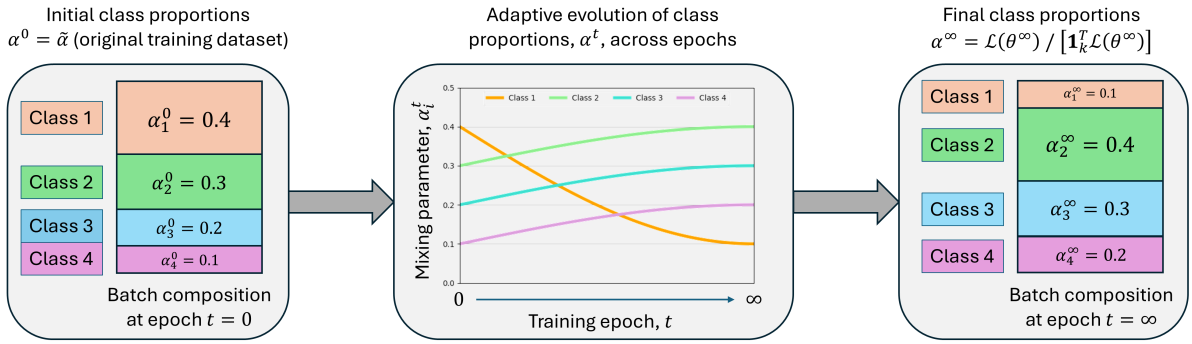


Figure 1: Illustration of the learn2mix training mechanism. The class-wise composition of batches is adaptively modified during training using instantaneous class-wise error rates.

This observation motivates the central question of this paper: *Can we dynamically adjust the proportion of classes within batches, across training epochs, to accelerate model convergence?* Addressing this question involves developing strategies that dynamically modify the proportion of classes using real-time performance metrics, thereby directing the learning procedure towards more challenging or underperforming classes. Such adaptive batch construction has the potential to enhance convergence rates and model accuracy, providing more efficient training, especially within scenarios characterized by class imbalance or heterogeneous class difficulties [Liu et al., 2008, Ren et al., 2018].

To address these considerations, in this work, we introduce *learn2mix*, a novel training strategy that dynamically modifies class proportions in batches by emphasizing classes with higher instantaneous error rates. In contrast with classical training schemes that utilize fixed class proportions, learn2mix continually adapts these proportions during training via real-time class-wise error metrics. This dynamic adjustment facilitates faster convergence and improved performance across various tasks, including classification, regression, and reconstruction. An illustration of the learn2mix training methodology is provided in Figure 1, demonstrating the adaptive class-wise composition of batches.

This paper is organized as follows. In Section 2, we formalize learn2mix, and prove relevant properties. In Section 3, we detail the algorithmic implementation of the learn2mix training methodology. In Section 4, we present empirical evaluations on benchmark datasets, demonstrating the efficacy of learn2mix in accelerating model convergence and enhancing performance. Finally, in Section 5, we summarize our paper. Our main contributions are outlined as follows:

1. We propose *learn2mix*, a novel adaptive training strategy that dynamically adjusts class proportions within batches, utilizing class-wise error rates, to accelerate model convergence in resource constrained regimes.
2. We prove that neural networks trained using *learn2mix* converge faster than those trained using classical ap-

proaches when certain properties hold, wherein the class proportions converge to a stable distribution proportional to the optimal class-wise error rates.

3. We empirically validate that neural networks trained using *learn2mix* consistently observe accelerated convergence, outperforming existing training methods in terms of convergence speed across classification, regression, and reconstruction tasks.

Related Work. The landscape of neural network training methods is characterized by a diverse set of approaches aiming to enhance model performance and training efficiency. Handling class imbalance has been extensively analyzed, with methods including oversampling [Chawla et al., 2002], undersampling [Tahir et al., 2012], and class-balanced loss functions [Lin et al., 2017, Ren et al., 2018] being proposed to mitigate biases towards majority classes. In parallel, curriculum learning [Bengio et al., 2009] and reinforcement learning-centric approaches [Florensa et al., 2017] have introduced methods to facilitate more effective learning trajectories. Meta-learning, or *learn2learn* methodologies [Arnold et al., 2020], including model-agnostic meta-learning (MAML) [Finn et al., 2017], focus on optimizing the learning process itself to enable rapid adaptation to new tasks, highlighting the importance of adaptability in model training. Additionally, adaptive data sampling strategies [Liu et al., 2008] and boosting algorithms [Freund and Schapire, 1997] emphasize the significance of prioritizing harder or misclassified examples to improve model robustness and convergence rates. Despite these advances, most existing training approaches either adjust sample weights, resample datasets, or modify the sequence of training examples without specifically altering the class proportions within batches in an adaptive manner. Our proposed *learn2mix* strategy distinguishes itself by continually adapting class proportions in these batches throughout the training process, directly targeting classes with higher error rates to accelerate convergence. This approach characterizes a unified framework by addressing class imbalance and integrating adaptive training principles, enhancing training efficiency.

2 THEORETICAL RESULTS

Consider the two random variables $X \in \mathbb{R}^d$ and $Y \in \mathbb{R}^k$, wherein X denotes the feature vector, Y are the labels, and k is the number of classes. We consider the *original training dataset*, $J = \{(x_j, y_j)\}_{j=1}^N$, where $(x_j, y_j) \stackrel{\text{i.i.d.}}{\sim} (X, Y)$, $\forall j \in \{1, \dots, N\}$. The class proportions for this dataset are given by the vector of fixed-proportion mixing parameters, $\tilde{\alpha} = [\tilde{\alpha}_1, \dots, \tilde{\alpha}_k]^T$, which reflects the distribution of classes. We define $\alpha = [\alpha_1, \dots, \alpha_k]^T$ as a variable denoting the vector of *mixing parameters*, where $\alpha_i \in [0, 1]$ and $\sum_{i=1}^k \alpha_i = 1$. The value of α determines the class proportions utilized during training, and can vary depending on the chosen training mechanism. In *classical training*, $\alpha = \alpha^t$ is constant over time and reflects the class proportions within the original training dataset, wherein $\alpha^t = \tilde{\alpha}$, $\forall t \in \mathbb{N}$. In *learn2mix training*, $\alpha = \alpha^t$ is time-varying, and is initialized at time $t = 0$ as $\alpha^0 = \tilde{\alpha}$.

Let $\mathcal{H} \subset \{h : \mathbb{R}^d \rightarrow \mathbb{R}^k\}$ be the class of hypothesis functions that model the relationship between X and Y . For our empirical setting, we let \mathcal{H} denote the set of neural networks that have predetermined architectures. We note \mathcal{H} is fully defined by a vector of parameters, $\theta \in \mathbb{R}^m$, where $\mathcal{H} = h_\theta$ denotes a set of parameterized functions. The generalized form of the loss function for classical training and the loss function form under learn2mix training are given below.

Definition 2.1 (Loss Function for Classical Training). Consider $\tilde{\alpha} \in [0, 1]^k$ as the vector of fixed-proportion mixing parameters, and let $\mathcal{L}(\theta^t) \in \mathbb{R}^k$ be the vector of class-wise losses at time t . The loss for classical training at time t is:

$$\mathcal{L}(\theta^t, \tilde{\alpha}) = \sum_{i=1}^k \tilde{\alpha}_i \mathcal{L}_i(\theta^t) = \tilde{\alpha}^T \mathcal{L}(\theta^t). \quad (1)$$

Definition 2.2 (Loss Function for Learn2Mix Training). Consider $\alpha^t, \alpha^{t-1} \in [0, 1]^k$ as the vector of mixing parameters at time t and time $t - 1$, and let $\mathcal{L}(\theta^t), \mathcal{L}(\theta^{t-1}) \in \mathbb{R}^k$ denote the respective class-wise loss vectors at time t and time $t - 1$. Consider $\gamma \in (0, 1)$ as the mixing rate. The loss for learn2mix training at time t is:

$$\mathcal{L}(\theta^t, \alpha^t) = \sum_{i=1}^k \alpha_i^t \mathcal{L}_i(\theta^t) = (\alpha^t)^T \mathcal{L}(\theta^t), \quad (2)$$

$$\text{Where: } \alpha^t = \alpha^{t-1} + \gamma \left(\frac{\mathcal{L}(\theta^{t-1})}{\mathbb{1}_k^T \mathcal{L}(\theta^{t-1})} - \alpha^{t-1} \right). \quad (3)$$

Suppose that \mathcal{H} is sufficiently expressive and can represent the true conditional expectation function, wherein there exists $\theta^* \in \mathbb{R}^m$ with $h_{\theta^*}(X) = \mathbb{E}[Y | X]$ almost surely. In the following proposition, we demonstrate that via gradient-based optimization under learn2mix training, the parameters converge to θ^* , with the mixing proportions converging to a stable distribution that reflects the relative difficulty of each class under the optimal parameters.

Proposition 2.3. Let $\mathcal{L}(\theta^t), \mathcal{L}(\theta^*) \in \mathbb{R}^k$ denote the class-wise loss vectors for the model parameters at time t and the optimal model parameters. Suppose each class-wise loss $\mathcal{L}_i(\theta) \in \mathbb{R}$ is strongly convex in θ , with strong convexity parameter $\mu_i \in \mathbb{R}_{>0}$, $\forall i \in \{1, \dots, k\}$, and each class-wise loss gradient $\nabla_\theta \mathcal{L}_i(\theta) \in \mathbb{R}^m$ is Lipschitz continuous in θ , having Lipschitz constant $L_i \in \mathbb{R}_{\geq 0}$, $\forall i \in \{1, \dots, k\}$. Let $\mu^* = \min_{i \in \{1, \dots, k\}} \mu_i$, $L^* = \max_{i \in \{1, \dots, k\}} L_i$. Then, if the model parameters at time $t + 1$ are obtained via the gradient of the loss for learn2mix training, where:

$$\theta^{t+1} = \theta^t - \eta \nabla_\theta \mathcal{L}(\theta^t, \alpha^t), \quad \text{with: } \eta \in \mathbb{R}_{>0}, \quad (4)$$

It follows that for learning rate, $\eta \in (0, 2/L^*)$, and for mixing rate, $\gamma \in (0, 1)$:

$$\lim_{t \rightarrow \infty} \theta^t = \theta^*, \quad \text{and: } \lim_{t \rightarrow \infty} \alpha^t = \alpha^* = \frac{\mathcal{L}(\theta^*)}{\mathbb{1}_k^T \mathcal{L}(\theta^*)}. \quad (5)$$

The complete proof of Proposition 2.3 is provided in Section A of the Appendix. We now detail the convergence behavior of the learn2mix and classical training strategies, and suppose that $\alpha^{t-1} = \tilde{\alpha}$. We first present Corollary 2.4, which will be used to prove the convergence result in Proposition 2.5. This corollary leverages Lipschitz continuity and strong convexity to bound the loss gradient norm.

Corollary 2.4. Let $\mathcal{L}(\theta^t) \in \mathbb{R}^k$ denote the class-wise loss vector at time t . Suppose each class-wise loss, $\mathcal{L}_i(\theta) \in \mathbb{R}$, is strongly convex in θ , with strong convexity parameter $\mu_i \in \mathbb{R}_{>0}$, $\forall i \in \{1, \dots, k\}$, and suppose each class-wise loss gradient $\nabla_\theta \mathcal{L}_i(\theta) \in \mathbb{R}^m$ is Lipschitz continuous in θ with Lipschitz constant $L_i \in \mathbb{R}_{\geq 0}$, $\forall i \in \{1, \dots, k\}$. Let $\mu^* = \min_{i \in \{1, \dots, k\}} \mu_i$, $L^* = \max_{i \in \{1, \dots, k\}} L_i$. Then, the following holds, $\forall \alpha \in [0, 1]^k$, with $\sum_{i=1}^k \alpha_i = 1$:

$$\frac{\mu^*}{2} \|\theta^t - \theta^*\| \leq \|\nabla_\theta \mathcal{L}(\theta^t, \alpha)\| \leq L^* \|\theta^t - \theta^*\|, \quad (6)$$

$$\|\nabla_\theta \mathcal{L}(\theta^t, \alpha^t)\| + \|\nabla_\theta \mathcal{L}(\theta^t, \tilde{\alpha})\| \leq 2L^* \|\theta^t - \theta^*\|. \quad (7)$$

The proof of Corollary 2.4 is provided in Section A of the Appendix — we note that the inequality in Eq. (7) relates the loss gradient norm under classical training with that under learn2mix training. We now present Proposition 2.5, which demonstrates that under the condition expressed in Eq. (8), updates obtained via the gradient of the loss for learn2mix training bring the model parameters closer to the optimal solution than those obtained via the gradient of the loss for classical training.

Proposition 2.5. Let $\mathcal{L}(\theta^t), \mathcal{L}(\theta^*) \in \mathbb{R}^k$ denote the respective class-wise loss vectors for the model parameters at time t and for the optimal model parameters. Suppose each class-wise loss, $\mathcal{L}_i(\theta) \in \mathbb{R}$ is strongly convex in θ with strong convexity parameter $\mu_i \in \mathbb{R}_{>0}$, $\forall i \in \{1, \dots, k\}$, and each class-wise loss gradient $\nabla_\theta \mathcal{L}_i(\theta) \in \mathbb{R}^m$ is Lipschitz continuous in θ , having Lipschitz constant $L_i \in \mathbb{R}_{\geq 0}$,

$\forall i \in \{1, \dots, k\}$. Moreover, suppose that the loss gradient $\nabla_{\theta} \mathcal{L}(\theta, \alpha) \in \mathbb{R}^m$ is Lipschitz continuous in α , having Lipschitz constant $L_{\alpha} \in \mathbb{R}_{\geq 0}$, and let $\mu^* = \min_{i \in \{1, \dots, k\}} \mu_i$, $L^* = \max_{i \in \{1, \dots, k\}} L_i$. Then, iff the following holds:

$$\left[\left(\frac{\mu^*}{2} - L^* \right) \|\theta^t - \theta^*\|^2 + \tilde{\alpha}^T (\mathcal{L}(\theta^t) - \mathcal{L}(\theta^*)) \right] \times \left[\|\theta^t - \theta^*\| - (\mathcal{L}(\theta^t) - \mathcal{L}(\theta^*)) \right] > 0, \quad (8)$$

It follows that for every learning rate, $\eta > 0$, and for every mixing rate, $\gamma \in (0, \beta]$:

$$\|(\theta^t - \eta \nabla_{\theta} \mathcal{L}(\theta^t, \alpha^t)) - \theta^*\| \leq \|(\theta^t - \eta \nabla_{\theta} \mathcal{L}(\theta^t, \tilde{\alpha})) - \theta^*\| \quad (9)$$

The formula for β can be found in Section A of the Appendix.

The complete proof of Proposition 2.5 is provided in Section A of the Appendix.

3 ALGORITHM

In this section, we outline our approach for training neural networks using learn2mix. The learn2mix mechanism consists of a bilevel optimization procedure, where we first update the parameters of the neural network, θ^t , and then modify the mixing parameters, α^t , using the vector of class-wise losses, $\mathcal{L}(\theta^t)$. Deriving from the original training dataset, J , consider $J_i = \{(x_j, y_j)\}_{j=1}^{\alpha_i N}$, $\forall i \in \{1, \dots, k\}$ as each class-specific training dataset, wherein $J = \bigcup_{i=1}^k J_i$. These k class-specific training datasets are leveraged to speed up batch construction under learn2mix, as we will subsequently delineate. We consider the case of training a neural network using batched stochastic gradient descent, such that for a given training epoch, t , the empirical loss is computed over $P = N/M$ total batches, where $M \in \mathbb{Z}^+$ denotes the batch size. Each batch is formed by sampling $\alpha_i^t M$ distinct examples from the i th class-specific training dataset, denoted as $S_i^p \subseteq J_i$, for $S^p = \biguplus_{i=1}^k S_i^p$. We let \biguplus denote the set union operator that preserves duplicate elements. For learn2mix training, the class-wise errors, $\mathcal{L}_i(\theta^t)$, $\forall i \in \{1, \dots, k\}$, at training epoch t are empirically computed as:

$$\mathcal{L}_i(\theta^t) = \frac{1}{P} \sum_{p=1}^P \left[\frac{1}{\alpha_i^t M} \sum_{(x_j, y_j) \in S_i^p} \ell(h_{\theta^t}(x_j), y_j) \right], \quad (10)$$

Where $\ell : \mathcal{Y} \times \mathcal{Y} \rightarrow \mathbb{R}_{\geq 0}$ is a bounded per-sample loss function and computes the error between the model prediction, $h_{\theta^t}(x_j)$, and the true label, y_j . Accordingly, the overall empirical loss at training epoch, t , under the learn2mix training mechanism is given by:

$$\begin{aligned} \mathcal{L}(\theta^t, \alpha^t) &= \sum_{i=1}^k \alpha_i^t \mathcal{L}_i(\theta^t) \\ &= \sum_{i=1}^k \alpha_i^t \left[\frac{1}{P} \sum_{p=1}^P \left[\frac{1}{\alpha_i^t M} \sum_{(x_j, y_j) \in S_i^p} \ell(h_{\theta^t}(x_j), y_j) \right] \right]. \end{aligned} \quad (11)$$

Algorithm 1: Neural Network Training Via Learn2Mix

Input: J (Original Training Dataset), θ (Initial NN Parameters), $\tilde{\alpha}$ (Initial Mixing Parameters), η (Learning Rate), γ (Mixing Rate), M (Batch Size), P (No. of Batches), E (Epochs)

Output: θ (Trained NN Parameters)

```

1 for  $i = 1, 2, \dots, k$  do
2    $J_i \leftarrow \{(x_j, y_j)\}_{j=1}^{\alpha_i N}$  (Initialize class-specific
   training datasets)
3    $\alpha_i \leftarrow \tilde{\alpha}_i$  (Initialize time-varying mixing params)
4 for  $epoch = 1, 2, \dots, E$  do
5   for  $i = 1, 2, \dots, k$  do
6      $J_i \leftarrow \text{Shuffle}(J_i)$  (Randomly shuffle each
     class-specific training dataset)
7   for  $p = 1, 2, \dots, P$  do
8     for  $i = 1, 2, \dots, k$  do
9        $S_i^p \leftarrow \text{Sample}(J_i, \alpha_i M)$  (Select  $\alpha_i M$ 
9       distinct examples from  $J_i$ )
10     $S^p \leftarrow \biguplus_{i=1}^k S_i^p$  (Aggregate to form batch  $S^p$ )
11     $\mathcal{L}^p(\theta, \alpha) \leftarrow \frac{1}{M} \sum_{(x_j, y_j) \in S^p} \ell(h_{\theta}(x_j), y_j)$ 
11    (Compute loss on batch  $S^p$ )
12     $\mathcal{L}(\theta, \alpha) \leftarrow \frac{1}{P} \sum_{p=1}^P \mathcal{L}^p(\theta, \alpha)$  (Obtain total loss)
13     $\theta \leftarrow \theta - \eta \nabla_{\theta} \mathcal{L}(\theta, \alpha)$  (Update model params,  $\theta$ )
14    for  $i = 1, 2, \dots, k$  do
15       $\mathcal{L}_i(\theta) \leftarrow$ 
15       $\frac{1}{P} \sum_{p=1}^P \frac{1}{\alpha_i M} \sum_{(x_j, y_j) \in S_i^p} \ell(h_{\theta}(x_j), y_j)$ 
15      (Compute loss for class  $i$ )
16     $\alpha \leftarrow \text{Update\_Mixing\_Params}(\alpha, \mathcal{L}(\theta), \gamma)$ 
17 return  $\theta$ 

```

Utilizing the empirical loss formulation from Eq. (11), we now detail the algorithmic implementation of the learn2mix training methodology on a per-sample basis, for consistency with the mathematical preliminaries in Section 2. We note that the batch processing equivalent of this procedure is a trivial extension to the domain of matrices, and was used to generate the empirical results from Section 4. Algorithm 1 outlines the primary training loop, where for each epoch, the class-specific datasets, J_i , are shuffled. Within each epoch, we iterate over the P total batches, forming each batch by choosing $\alpha_i M$ examples from every J_i . The empirical loss within each batch is computed and aggregated to obtain the overall loss, $\mathcal{L}(\theta, \alpha)$, which is then used to update the neural network parameters through gradient descent. Lastly, the vector of class-wise losses, $\mathcal{L}(\theta)$, is calculated to inform the adjustment of the mixing parameters, α , using Algorithm 2.

Algorithm 2 encapsulates the mechanism for adjusting class proportions via the mixing parameters, α , based on the computed class-wise losses. For each class, $i \in \{1, \dots, k\}$, the algorithm normalizes the class-wise loss, $\mathcal{L}_i(\theta)$, by the cumulative loss across classes to obtain L_i . The mixing pa-

Algorithm 2: Updating Mixing Params Via Learn2Mix

Input: α (Previous Mixing Parameters), $\mathcal{L}(\theta)$ (Class-wise loss vector), γ (Mixing Rate)

Output: α (Updated Mixing Parameters)

```

1 for  $i = 1, 2, \dots, k$  do
2    $L_i \leftarrow \frac{\mathcal{L}_i(\theta)}{\sum_{j=1}^k \mathcal{L}_j(\theta)}$  (Compute normalized losses)
3    $\alpha_i \leftarrow \alpha_i + \gamma (L_i - \alpha_i)$  (Update mixing params)
4 return  $\alpha$ 

```

parameter α_i is then updated by moving it towards L_i , with the step size controlled by the mixing rate, γ . This adaptive update ensures that classes with higher error rates receive increased attention in subsequent epochs, promoting balanced and focused learning across all classes.

Finally, we recall that during the batch construction phase, for each class, $i \in \{1, \dots, k\}$, we select $\alpha_i M$ examples from each J_i to form the subset $S_i^p \subseteq J_i$. Given the dynamic nature of the mixing parameters, α , it is possible that this cumulative selection across batches may exhaust all the samples within a particular J_i before the epoch concludes. To address this, we incorporate a cyclic selection mechanism. Formally, we define an index $\tau_i^p, \forall i \in \{1, \dots, k\}$ and $p \in \{1, \dots, P\}$, such that:

$$\tau_i^p = \left(\tau_i^{p-1} + \alpha_i M \right) \bmod \tilde{\alpha}_i N, \quad (12)$$

Where $\tau_i^0 = 0, \forall i \in \{1, \dots, k\}$. Accordingly, when selecting S_i^p , if $\tau_i^{p-1} + \alpha_i M > \tilde{\alpha}_i N$, we wrap around to the beginning of J_i , effectively resetting the selection index, τ_i^p — this ensures that every example in J_i is selected uniformly and repeatedly as needed throughout the training process. Thus, the selection procedure to construct S_i^p is defined as:

$$S_i^p = \bigcup_{w=0}^{\alpha_i M - 1} J_i \left[(\tau_i^{p-1} + w) \bmod \tilde{\alpha}_i N \right]. \quad (13)$$

This cyclic selection procedure ensures that the required number of samples, $\alpha_i M$, for each class in every batch is maintained, even as α_i is adaptively updated across epochs.

4 EMPIRICAL RESULTS

In this section, we present our empirical results on classification, regression, and image reconstruction tasks, across both benchmark and modified class imbalanced datasets. We first present the classification results on three benchmark datasets (MNIST [Deng, 2012], Fashion-MNIST [Xiao et al., 2017], CIFAR-10 [Krizhevsky et al., 2009]), and three standard datasets with manually imbalanced classes (Imagenette [Howard, 2020], CIFAR-100 [Krizhevsky et al., 2009], and IMDB [Maas et al., 2011]). We note that for

the imbalanced case, we only introduce the manual class-imbancing to the training dataset, J , where the test dataset, $K = \{(x_j, y_j)\}_{j=1}^{N_{\text{test}}}$, is not changed. This choice ensures that the generalization performance of the network is benchmarked in a class-balanced setting. Next, for the regression task, we study two benchmark datasets with manually imbalanced classes (Wine Quality [Cortez et al., 2009], and California Housing [Géron, 2022]), and a synthetic mean estimation task, wherein the manual class-imbancing parallels that of the classification case. Finally, we reconsider the MNIST, Fashion MNIST and CIFAR-10 datasets in the context of image reconstruction, again considering the aforementioned manual class-imbancing procedure. A comprehensive description of these datasets and class-imbancing strategies is provided in Section B of the Appendix.

The intuition behind the application of learn2mix to regression and reconstruction tasks stems from its ability to adaptively handle different data distributions. As an example, for regression tasks involving a categorical variable taking k distinct values, the samples from the original training dataset, J , that correspond to each of these k values, can be aggregated to obtain each class-specific training dataset, J_i . Here, each dataset, J_i , represents a different underlying distribution. Paralleling the classification case, learn2mix will adaptively adjust the proportions of the class-specific datasets during training. Similarly, in the context of image reconstruction, we can treat the k distinct classes being reconstructed as the values taken by a categorical variable, paralleling the regression context. This formulation supports the adaptive adjustment of class proportions under learn2mix training.

For the evaluations that follow, to ensure a fair comparison between the learn2mix training strategy and the classical training strategy, we use the same learning rate, η , and neural network architecture with initialized parameters, θ , across all experiments for a given dataset. Additionally, we train each neural network through learn2mix (with mixing rate γ) and classical training for E training epochs, where E is dataset and task dependent¹. In classification tasks, we also benchmark learn2mix and classical training versus ‘focal training’ and ‘SMOTE training’ (training using focal loss [Lin et al., 2017] and SMOTE oversampling [Chawla et al., 2002] — see Sections C.2 and C.3 of the Appendix). The complete list of model architectures and hyperparameter choices is provided in Section C of the Appendix.

4.1 CLASSIFICATION TASKS

As illustrated in Table 1 and Figure 2, we observe a consistent trend across all considered classification benchmarks, whereby neural networks trained using learn2mix converge faster than their classically-trained, focal loss-trained, and SMOTE-trained counterparts. More concretely, we begin by

¹Practically, we observe that choosing $\gamma \in [0.01, 0.5]$ yields improved performance (see empirical results).

Table 1: Test classification accuracy for learn2mix (L2M), classical (CL), focal (FCL), SMOTE training.

Epoch $t = 0.25E$						
Dataset	MNIST	Fashion MNIST	CIFAR-10	Imagenette	CIFAR-100	IMDB
Accuracy (L2M)	77.62 \pm 1.83	46.52 \pm 3.25	51.38 \pm 0.40	33.89 \pm 1.66	7.270 \pm 0.46	70.82 \pm 1.69
Accuracy (CL)	66.07 \pm 4.57	40.54 \pm 3.43	49.89 \pm 0.51	25.16 \pm 1.01	4.600 \pm 0.32	53.82 \pm 3.93
Accuracy (FCL)	69.92 \pm 4.71	40.59 \pm 3.42	49.59 \pm 0.70	27.63 \pm 2.15	6.836 \pm 0.27	50.89 \pm 1.10
Accuracy (SMOTE)	67.87 \pm 5.23	40.43 \pm 3.47	50.08 \pm 0.53	29.76 \pm 0.72	6.570 \pm 0.42	54.38 \pm 2.41
Epoch $t = 0.5E$						
Dataset	MNIST	Fashion MNIST	CIFAR-10	Imagenette	CIFAR-100	IMDB
Accuracy (L2M)	85.04 \pm 1.38	60.12 \pm 1.30	56.76 \pm 0.69	43.50 \pm 0.86	12.10 \pm 0.36	76.12 \pm 2.36
Accuracy (CL)	82.69 \pm 1.58	54.59 \pm 3.11	55.36 \pm 0.40	33.72 \pm 1.24	8.200 \pm 0.26	72.32 \pm 3.28
Accuracy (FCL)	83.46 \pm 1.52	56.09 \pm 2.56	54.81 \pm 0.43	35.82 \pm 0.97	11.12 \pm 0.40	69.33 \pm 3.89
Accuracy (SMOTE)	82.93 \pm 1.67	54.55 \pm 3.10	54.76 \pm 0.68	38.73 \pm 0.47	10.86 \pm 0.47	66.28 \pm 1.78
Epoch $t = E$						
Dataset	MNIST	Fashion MNIST	CIFAR-10	Imagenette	CIFAR-100	IMDB
Accuracy (L2M)	91.18 \pm 1.03	67.34 \pm 1.18	62.10 \pm 0.39	53.31 \pm 0.68	17.02 \pm 0.48	82.33 \pm 0.50
Accuracy (CL)	90.01 \pm 1.12	65.27 \pm 1.74	61.46 \pm 0.31	44.60 \pm 0.68	12.62 \pm 0.37	80.03 \pm 0.48
Accuracy (FCL)	90.08 \pm 1.07	66.32 \pm 1.71	61.19 \pm 0.18	45.30 \pm 0.74	14.45 \pm 0.57	79.83 \pm 0.71
Accuracy (SMOTE)	90.08 \pm 1.13	65.27 \pm 1.73	60.93 \pm 0.25	49.41 \pm 0.73	15.05 \pm 0.61	77.46 \pm 0.70

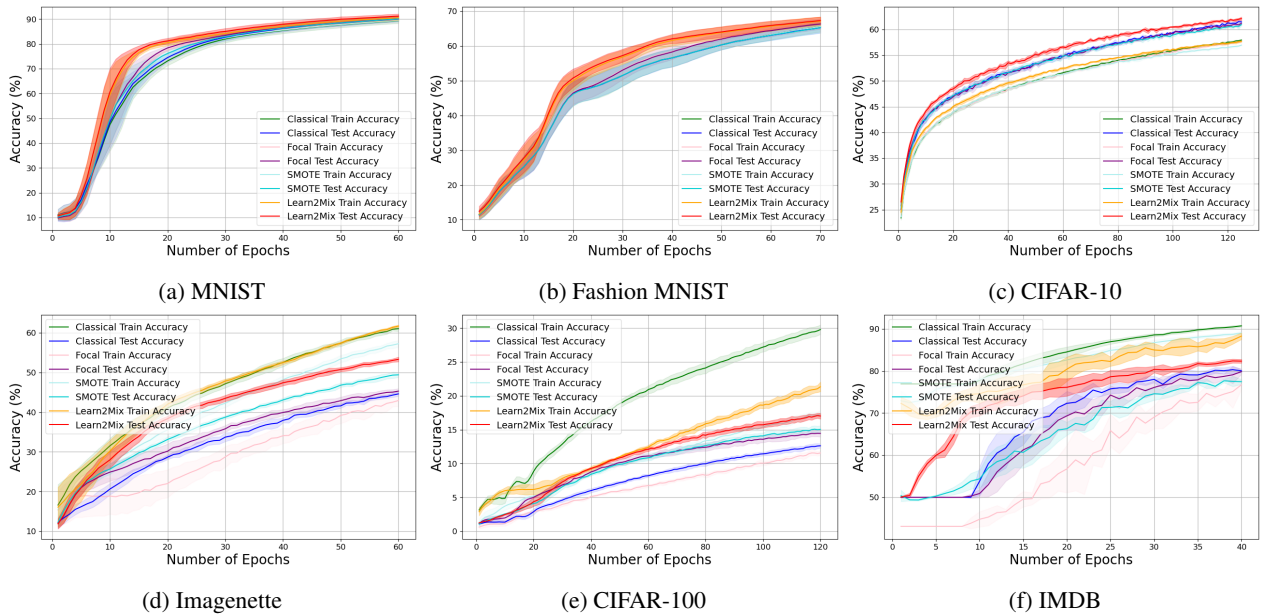


Figure 2: Comparing model classification accuracies across six datasets (MNIST, Fashion MNIST, CIFAR-10, Imagenette, CIFAR-100, IMDB Sentiment Analysis) using Cross Entropy Loss for classical training, learn2mix training, focal training, and SMOTE training. The x-axis is the number of elapsed training epochs, while the y-axis is the classification accuracy.

considering the MNIST benchmark dataset. We train LeNet-5 [Lecun et al., 1998] via the Adam optimizer [Kingma and Ba, 2014] and Cross Entropy Loss for $E = 60$ epochs on MNIST, leveraging learn2mix, classical, focal, and SMOTE training. We note that the learn2mix-trained CNN achieves faster convergence, eclipsing a test accuracy of 75% after 14 epochs, whereas the respective classically-trained, focal loss-trained, and SMOTE-trained CNNs achieve this test accuracy after 20 epochs, 18 epochs, and 19 epochs. Subsequently, we consider the more challenging Fashion MNIST benchmark dataset. We train LeNet-5 for $E = 70$

epochs with the Adam optimizer and Cross Entropy Loss on Fashion MNIST, leveraging learn2mix, classical, focal, and SMOTE training. Paralleling the MNIST case, we observe that the learn2mix-trained CNN achieves faster convergence, yielding a test accuracy of 60% after 35 epochs, whereas the respective classically-trained, focal loss-trained, and SMOTE-trained CNNs achieve this test accuracy after 49 epochs, 44 epochs, and 49 epochs. The last class-balanced benchmark dataset we investigate is the CIFAR-10 dataset, which offers a greater challenge than MNIST and Fashion MNIST. We train LeNet-5 for $E = 125$ epochs using the

Adam optimizer and Cross Entropy Loss on CIFAR-10, utilizing learn2mix, classical, focal, and SMOTE training. We observe that the learn2mix-trained CNN achieves faster convergence, yielding a test accuracy of 55% after 50 epochs, whereas the respective classically-trained, focal loss-trained, and SMOTE-trained CNNs exceed this test accuracy after 60 epochs, 61 epochs, and 60 epochs. Cumulatively, these evaluations demonstrate the efficacy of learn2mix training in settings with balanced classes, wherein the adaptive adjustment of class proportions accelerates convergence.

We now consider the case of benchmarking classification accuracies when the training dataset consists of imbalanced classes. We first benchmark the Imagenette dataset, which is characterized by a subset of 10 classes from ImageNet [Deng et al., 2009], and modify the training dataset such that the number of samples from each class, $i \in \{1, \dots, k\}$, in J decreases linearly. We train ResNet-18 [He et al., 2016] utilizing the Adam optimizer and Cross Entropy Loss for $E = 60$ epochs on Imagenette, via learn2mix, classical, focal, and SMOTE training. We observe that the learn2mix-trained ResNet-18 model converges faster, achieving a test accuracy of 40% after 22 epochs, at which point the respective classically-trained, focal loss-trained, and SMOTE-trained ResNet-18 models have test accuracies of 30%, 32% and 35%. Next, we consider the CIFAR-100 dataset, and again modify the training dataset such that the number of samples from each class, $i \in \{1, \dots, k\}$, in J decreases logarithmically. We train LeNet-5 for $E = 120$ epochs using the Adam optimizer and Cross Entropy Loss on CIFAR-100, via learn2mix, classical, focal, and SMOTE training. We see that the learn2mix-trained LeNet-5 model observes faster convergence, achieving a test accuracy of 15% after 90 epochs, at which point the respective classically-trained, focal loss-trained, and SMOTE-trained CNNs have test accuracies of 11% and 13.3%, and 13.4%. We further note that the $k = 100$ mixing parameters within learn2mix are a small fraction of the total model parameters, making this overhead negligible. Regarding the IMDB dataset, we modify the training dataset such that the positive class keeps 30% of its original samples. We train a transformer for $E = 40$ epochs utilizing the Adam optimizer and Cross Entropy Loss on IMDB, with learn2mix, classical, focal, and SMOTE training. We find that the learn2mix-trained transformer converges faster, reaching a test accuracy of 75% after 16 epochs, at which point the respective classically-trained, focal loss-trained, and SMOTE-trained transformers have test accuracies of 68%, 62%, and 61.8%. These experiments demonstrate the efficacy of learn2mix training over existing approaches in imbalanced classification settings.

In the class-imbalance evaluations, we see that learn2mix not only accelerates convergence, but also achieves a tighter alignment between training and test errors compared to classical training. This correspondence indicates reduced overfitting, as learn2mix inherently adjusts class propor-

tions based on class-specific error rates, L_i . By biasing the optimization procedure away from the original class distribution and towards L_i , learn2mix improves the model’s generalization performance. We note that this property is not unique to classification and also applies to regression and reconstruction (see Sections 4.2 and 4.3).

4.2 REGRESSION TASKS

As illustrated in Table 2 and Figure 3, we observe that learn2mix maintains accelerated convergence in the regression context, wherein all the considered datasets are class imbalanced. We first consider the synthetic Mean Estimation dataset, which comprises sets of samples gathered from $k = 4$ unique distributions and their associated means. Using the Adam optimizer and Mean Squared Error (MSE) Loss, we train a fully connected network for $E = 500$ epochs on Mean Estimation via learn2mix and classical training. We see that the learn2mix-trained neural network observes rapid convergence, achieving a test error below 2.0 after 100 epochs, at which point the classically-trained network has a test error of 13.0. For the Wine Quality dataset, we modify the training dataset such that the white wine class has 10% of its original samples. Utilizing the Adam optimizer and MSE Loss, we train a fully connected network for $E = 300$ epochs on Wine Quality via learn2mix and classical training. We observe that the learn2mix-trained neural network yields faster convergence, achieving a test error below 2.5 after 200 epochs, at which point the classically-trained network has a test error of 5.0. Finally, on the California Housing dataset, we modify the training dataset such that three of the classes have 5% of their original samples. Using the Adam optimizer and MSE Loss, we train a fully connected network for $E = 1200$ epochs on California Housing via learn2mix and classical training. We again see that the learn2mix-trained network converges faster, achieving a test error below 0.8 after 1200 epochs, while the classically-trained network has a test error of 0.99. These empirical evaluations support our previous intuition pertaining to the extension of learn2mix to imbalanced regression settings.

4.3 IMAGE RECONSTRUCTION TASKS

Per Table 2 and Figure 3, we note that the class-imbalanced image reconstruction tasks also observe faster convergence using learn2mix. For the MNIST case, we modify the training dataset such that half of the classes retain 20% of their original samples. Leveraging the Adam optimizer and MSE Loss, we train an autoencoder for $E = 40$ epochs on MNIST using learn2mix and classical training. We observe that the learn2mix-trained autoencoder exhibits improved convergence, achieving a test error less than 1.0 after 35 epochs, which the classically-trained autoencoder achieves after 40 epochs. Correspondingly, for Fashion MNIST, we modify the training dataset such that half of the classes retain 20%

Table 2: Test mean squared error (MSE) for learn2mix (L2M) and classical (CL) training.

Dataset	Epoch $t = 0.25E$		Epoch $t = 0.5E$		Epoch $t = E$	
	MSE (L2M)	MSE (CL)	MSE (L2M)	MSE (CL)	MSE (L2M)	MSE (CL)
Mean Estimation	1.81 ± 0.84	6.51 ± 1.52	1.45 ± 0.26	1.52 ± 0.27	1.07 ± 0.09	1.17 ± 0.06
Wine Quality	17.7 ± 1.64	19.8 ± 1.51	4.26 ± 1.55	9.72 ± 1.94	1.75 ± 0.21	2.03 ± 0.18
California Housing	2.52 ± 0.68	2.95 ± 0.67	1.33 ± 0.32	1.82 ± 0.39	0.77 ± 0.08	0.99 ± 0.10
MNIST	19.6 ± 0.81	20.8 ± 0.93	12.9 ± 0.39	14.0 ± 0.52	9.31 ± 0.24	10.1 ± 0.56
Fashion MNIST	89.3 ± 2.63	91.9 ± 2.37	65.1 ± 1.21	70.9 ± 1.28	45.5 ± 1.21	51.6 ± 1.60
CIFAR-10	193 ± 1.23	194 ± 1.98	175 ± 2.85	179 ± 3.87	144 ± 1.71	148 ± 1.37

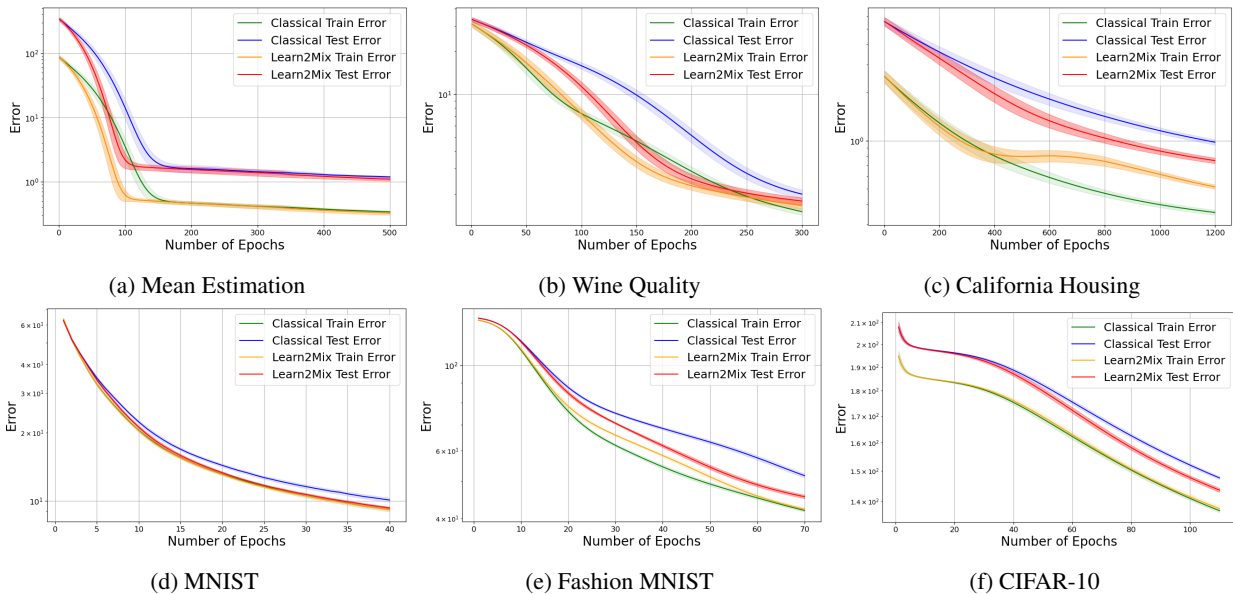


Figure 3: Comparing model performance errors across six datasets (Mean Estimation, Wine Quality, California Housing, MNIST, Fashion MNIST, CIFAR-10) using MSE Loss for classical training and learn2mix training. The x-axis is the number of elapsed training epochs, while the y-axis is the mean squared error (MSE).

of their original samples (paralleling MNIST). Using the Adam optimizer and MSE Loss, we train an autoencoder for $E = 70$ epochs on Fashion MNIST, leveraging learn2mix and classical training. We observe that the learn2mix-trained autoencoder converges faster, achieving a test error below 54.0 after 50 epochs, which the classically-trained autoencoder achieves after 65 epochs. We also consider CIFAR-10, wherein we modify the training dataset such that all but two classes retain 20% of their original samples. Utilizing the Adam optimizer and MSE Loss, we train an autoencoder for $E = 110$ epochs on CIFAR-10, leveraging learn2mix and classical training. We observe that the learn2mix-trained autoencoder also converges faster and achieves a test error below 148.0 after 100 epochs, which the classically-trained autoencoder achieves after 110 epochs. Cumulatively, these empirical evaluations demonstrate the improved performance yielded by learn2mix trained models over classically trained models in constrained training regimes.

5 CONCLUSION

In this work, we presented *learn2mix*, a new training strategy that adaptively modifies class proportions in batches via real-time class-wise error rates, accelerating model convergence. We formalized the learn2mix mechanism through a bilevel optimization framework, and outlined its theoretical advantages in aligning class proportions with optimal error rates. Empirical evaluations across classification, regression, and reconstruction tasks on both balanced and imbalanced datasets confirmed that learn2mix not only accelerates convergence compared to classical training methods, but also reduces overfitting in the presence of class-imbalances. As a consequence, models trained with learn2mix achieved improved performance in constrained training regimes. Our findings underscore the potential of dynamic batch composition strategies in optimizing neural network training, paving the way for more efficient and robust machine learning models in resource-constrained environments.

Acknowledgements

This work was supported in part by the U.S. Air Force Office of Scientific Research (AFOSR) under award FA8750-20-2-0504. Any opinions, findings and conclusions or recommendations expressed in this material are those of the authors and do not necessarily reflect the views of the U.S. Department of Defense.

References

- Sébastien M. R. Arnold, Praateek Mahajan, Debajyoti Datta, Ian Bunner, and Konstantinos Saitas Zarkias. learn2learn: A library for meta-learning research, 2020.
- Alexei Baevski, Henry Zhou, Abdelrahman Mohamed, and Michael Auli. wav2vec 2.0: A framework for self-supervised learning of speech representations. In *2020 IEEE International Conference on Acoustics, Speech and Signal Processing (ICASSP)*, pages 776–780. IEEE, 2020.
- Yoshua Bengio, Jean Louradour, Ronan Collobert, and Jason Weston. Curriculum learning. In *Proceedings of the 26th Annual International Conference on Machine Learning*, pages 41–48. ACM, 2009.
- Léon Bottou. Large-scale machine learning with stochastic gradient descent. In *Proceedings of COMPSTAT'2010*, pages 177–186. Springer, 2010.
- Mateusz Buda, Atsuto Maki, and Maciej A Mazurowski. A systematic study of the class imbalance problem in convolutional neural networks. *Neural Networks*, 106: 249–259, 2018.
- Nitesh V Chawla, Kevin W Bowyer, Lawrence O Hall, and W Philip Kegelmeyer. Smote: Synthetic minority over-sampling technique. In *Proceedings of the 2002 Joint Conference on IEEE International Conference on Knowledge Discovery and Data Mining and IEEE European Conference on Machine Learning*, pages 878–884. IEEE, 2002.
- Paulo Cortez, António Cerdeira, Fernando Almeida, Telmo Matos, and José Reis. Modeling wine preferences by data mining from physicochemical properties. *Decision support systems*, 47(4):547–553, 2009.
- Jia Deng, Wei Dong, Richard Socher, Li-Jia Li, Kai Li, and Li Fei-Fei. Imagenet: A large-scale hierarchical image database. In *2009 IEEE conference on computer vision and pattern recognition*, pages 248–255. Ieee, 2009.
- Li Deng. The mnist database of handwritten digit images for machine learning research. *IEEE Signal Processing Magazine*, 29(6):141–142, 2012.
- Jacob Devlin, Ming-Wei Chang, Kenton Lee, and Kristina Toutanova. Bert: Pre-training of deep bidirectional transformers for language understanding. *arXiv preprint arXiv:1810.04805*, 2018.
- Chelsea Finn, Pieter Abbeel, and Sergey Levine. Model-agnostic meta-learning for fast adaptation of deep networks. In Doina Precup and Yee Whye Teh, editors, *Proceedings of the 34th International Conference on Machine Learning*, volume 70 of *Proceedings of Machine Learning Research*, pages 1126–1135. PMLR, 06–11 Aug 2017.
- Carlos Florensa, Yoshua Bengio, and Aaron Courville. Automatic goal generation for reinforcement learning agents. In *International Conference on Learning Representations*, 2017.
- Yoav Freund and Robert E Schapire. A decision-theoretic generalization of on-line learning and an application to boosting. *Journal of computer and system sciences*, 55 (1):119–139, 1997.
- Aurélien Géron. *Hands-on machine learning with Scikit-Learn, Keras, and TensorFlow*. " O'Reilly Media, Inc.", 2022.
- Priya Goyal, Piotr Dollár, Ross Girshick, Pieter Noordhuis, Lukasz Wesolowski, Ari Kyrola, Joshua Tulloch, Yangqing Jia, and Kaiming He. Accurate, large mini-batch sgd: Training imagenet in 1 hour. In *Proceedings of the IEEE conference on computer vision and pattern recognition*, pages 1206–1214, 2017.
- Alex Graves, Marc G Bellemare, Jacob Menick, Remi Munos, and Koray Kavukcuoglu. Automated curriculum learning for neural networks. In *international conference on machine learning*, pages 1311–1320. Pmlr, 2017.
- Kaiming He, Xiangyu Zhang, Shaoqing Ren, and Jian Sun. Deep residual learning for image recognition. In *Proceedings of the IEEE Conference on Computer Vision and Pattern Recognition*, pages 770–778, 2016.
- Geoffrey Hinton, Li Deng, Dong Yu, George E Dahl, Abdelrahman Mohamed, Navdeep Jaitly, Andrew Senior, Vincent Vanhoucke, Patrick Nguyen, Tara N Sainath, et al. Deep neural networks for acoustic modeling in speech recognition: The shared views of four research groups. *IEEE Signal Processing Magazine*, 29(6):82–97, 2012.
- Jeremy Howard. Imagenette. <https://github.com/fastai/imagenette>, 2020.
- Sergey Ioffe and Christian Szegedy. Batch normalization: Accelerating deep network training by reducing internal covariate shift. In *International Conference on Machine Learning*, pages 448–456. PMLR, 2015.

- Diederik P Kingma and Jimmy Ba. Adam: A method for stochastic optimization. *arXiv preprint arXiv:1412.6980*, 2014.
- Alex Krizhevsky, Geoffrey Hinton, et al. Learning multiple layers of features from tiny images. 2009.
- Alex Krizhevsky, Ilya Sutskever, and Geoffrey E Hinton. Imagenet classification with deep convolutional neural networks. In *Advances in Neural Information Processing Systems*, pages 1097–1105, 2012.
- Y. Lecun, L. Bottou, Y. Bengio, and P. Haffner. Gradient-based learning applied to document recognition. *Proceedings of the IEEE*, 86(11):2278–2324, 1998. doi: 10.1109/5.726791.
- Tsung-Yi Lin, Priya Goyal, Ross Girshick, Kaiming He, and Piotr Dollar. Focal loss for dense object detection. In *Proceedings of the IEEE International Conference on Computer Vision*, pages 2980–2988, 2017.
- Xu-Ying Liu, Jianxin Wu, and Zhi-Hua Zhou. Exploratory undersampling for class-imbalance learning. *IEEE Transactions on Systems, Man, and Cybernetics, Part B (Cybernetics)*, 39(2):539–550, 2008.
- Andrew L. Maas, Raymond E. Daly, Peter T. Pham, Dan Huang, Andrew Y. Ng, and Christopher Potts. Learning word vectors for sentiment analysis. In *Proceedings of the 49th Annual Meeting of the Association for Computational Linguistics: Human Language Technologies*, pages 142–150, Portland, Oregon, USA, June 2011. Association for Computational Linguistics.
- Minlong Peng, Qi Zhang, Xiaoyu Xing, Tao Gui, Xuanjing Huang, Yu-Gang Jiang, Keyu Ding, and Zhigang Chen. Trainable undersampling for class-imbalance learning. In *Proceedings of the AAAI conference on artificial intelligence*, volume 33, pages 4707–4714, 2019.
- Lutz Prechelt. Early stopping - but when? In *Neural Networks: Tricks of the trade*, pages 55–69. Springer, 1998.
- Alec Radford, Jeffrey Wu, Rewon Child, David Luan, Dario Amodei, and Ilya Sutskever. Language models are unsupervised multitask learners. *OpenAI Blog*, 1(8), 2019.
- Mengye Ren, Wenyuan Zeng, Bin Yang, and Raquel Urtasun. Learning to reweight examples for robust deep learning. In *International conference on machine learning*, pages 4334–4343. PMLR, 2018.
- David E Rumelhart, Geoffrey E Hinton, and Ronald J Williams. Learning representations by back-propagating errors. *Nature*, 323(6088):533–536, 1986.
- Connor Shorten and Taghi M Khoshgoftaar. A survey on image data augmentation for deep learning. *Journal of Big Data*, 6(1):60, 2019.
- Karen Simonyan and Andrew Zisserman. Very deep convolutional networks for large-scale image recognition. *arXiv preprint arXiv:1409.1556*, 2014.
- Leslie N. Smith. Cyclical learning rates for training neural networks. In *2017 IEEE Winter Conference on Applications of Computer Vision (WACV)*, pages 464–472. IEEE, 2017.
- Nitish Srivastava, Geoffrey Hinton, Alex Krizhevsky, Ilya Sutskever, and Ruslan R Salakhutdinov. Dropout: A simple way to prevent neural networks from overfitting. *Journal of Machine Learning Research*, 15(1):1929–1958, 2014.
- Muhammad Atif Tahir, Josef Kittler, and Fei Yan. Inverse random under sampling for class imbalance problem and its application to multi-label classification. *Pattern Recognition*, 45(10):3738–3750, 2012.
- Hugo Touvron, Thibaut Lavril, Gautier Izacard, Xavier Martinet, Marie-Anne Lachaux, Timothée Lacroix, Baptiste Rozière, Naman Goyal, Eric Hambro, Faisal Azhar, Aurelien Rodriguez, Armand Joulin, Edouard Grave, and Guillaume Lample. Llama: Open and efficient foundation language models, 2023.
- Vladimir Vapnik and Léon Bottou. Local algorithms for pattern recognition and dependencies estimation. *Neural Computation*, 5(6):893–909, 1993.
- Ashish Vaswani, Noam Shazeer, Niki Parmar, Jakob Uszkoreit, Llion Jones, Aidan N Gomez, Łukasz Kaiser, and Illia Polosukhin. Attention is all you need. In *Advances in Neural Information Processing Systems*, pages 5998–6008, 2017.
- Xin Wang, Yudong Chen, and Wenwu Zhu. A survey on curriculum learning. *IEEE transactions on pattern analysis and machine intelligence*, 44(9):4555–4576, 2021.
- Xueyuan Wang and M Cenk Gursoy. Resilient path planning for uavs in data collection under adversarial attacks. *IEEE Transactions on Information Forensics and Security*, 18: 2766–2779, 2023.
- Yiru Wang, Weihao Gan, Jie Yang, Wei Wu, and Junjie Yan. Dynamic curriculum learning for imbalanced data classification. In *2019 IEEE/CVF International Conference on Computer Vision (ICCV)*, pages 5016–5025, 2019. doi: 10.1109/ICCV.2019.00512.
- Han Xiao, Kashif Rasul, and Roland Vollgraf. Fashion-mnist: a novel image dataset for benchmarking machine learning algorithms. *arXiv preprint arXiv:1708.07747*, 2017.

Appendix

Shyam Venkatasubramanian¹

Vahid Tarokh¹

¹Duke University, Durham, North Carolina, USA

A PROOFS OF THE THEORETICAL RESULTS

In this section, we present the proofs of the theoretical results outlined in the main text.

Proposition 2.3. *Let $\mathcal{L}(\theta^t), \mathcal{L}(\theta^*) \in \mathbb{R}^k$ denote the class-wise loss vectors for the model parameters at time t and the optimal model parameters. Suppose each class-wise loss $\mathcal{L}_i(\theta) \in \mathbb{R}$ is strongly convex in θ , with strong convexity parameter $\mu_i \in \mathbb{R}_{>0}, \forall i \in \{1, \dots, k\}$, and each class-wise loss gradient $\nabla_{\theta} \mathcal{L}_i(\theta) \in \mathbb{R}^m$ is Lipschitz continuous in θ , having Lipschitz constant $L_i \in \mathbb{R}_{\geq 0}, \forall i \in \{1, \dots, k\}$. Let $\mu^* = \min_{i \in \{1, \dots, k\}} \mu_i, L^* = \max_{i \in \{1, \dots, k\}} L_i$. Then, if the model parameters at time $t + 1$ are obtained via the gradient of the loss for learn2mix training, where:*

$$\theta^{t+1} = \theta^t - \eta \nabla_{\theta} \mathcal{L}(\theta^t, \alpha^t), \quad \text{with: } \eta \in \mathbb{R}_{>0}, \quad (14)$$

It follows that for learning rate, $\eta \in (0, 2/L^*)$, and for mixing rate, $\gamma \in (0, 1)$:

$$\lim_{t \rightarrow \infty} \theta^t = \theta^*, \quad \text{and: } \lim_{t \rightarrow \infty} \alpha^t = \alpha^* = \frac{\mathcal{L}(\theta^*)}{\mathbf{1}_k^T \mathcal{L}(\theta^*)}. \quad (15)$$

Proof. We begin by recalling that $\mathcal{L}_i(\theta)$ is strongly convex in θ with strong convexity parameter $\mu_i, \forall i \in \{1, \dots, k\}$. Accordingly, $\forall \alpha \in [0, 1]^k$, with $\sum_{i=1}^k \alpha_i = 1$, the loss function $\mathcal{L}(\theta, \alpha)$ is strongly convex in θ with parameter, $\mu' \in \mathbb{R}_{>0}$, which is lower bounded by $\mu^* \in \mathbb{R}_{>0}$, as per Eq. (16).

$$\mu' \geq \mu^* > 0, \quad \text{where: } \mu^* = \min_{i \in \{1, \dots, k\}} \mu_i, \quad \text{and: } \mu' = \sum_{i=1}^k \alpha_i \mu_i. \quad (16)$$

We note that this lower bound on the strong convexity parameter, $\mu' \geq \mu^*$, holds independently of α . Now, recall that $\nabla_{\theta} \mathcal{L}_i(\theta)$, is Lipschitz continuous in θ with Lipschitz constant $L_i, \forall i \in \{1, \dots, k\}$. Accordingly, $\forall \alpha \in [0, 1]^k$, where $\sum_{i=1}^k \alpha_i = 1$, the loss gradient $\nabla_{\theta} \mathcal{L}(\theta, \alpha)$ is Lipschitz continuous in θ with Lipschitz constant, $L' \in \mathbb{R}_{\geq 0}$, which is upper bounded by $L^* \in \mathbb{R}_{\geq 0}$, as per Eq. (17).

$$L^* \geq L' \geq 0, \quad \text{where: } L^* = \max_{i \in \{1, \dots, k\}} L_i, \quad \text{and: } L' = \sum_{i=1}^k \alpha_i L_i. \quad (17)$$

We affirm that this upper bound on the Lipschitz constant, $L' \leq L^*$, holds independently of α . Now, suppose that $\alpha = \alpha^t$, where $\mathcal{L}(\theta, \alpha^t)$ is strongly convex in θ with parameter $\mu' \geq \mu^*$ and $\nabla_{\theta} \mathcal{L}(\theta, \alpha^t)$ is Lipschitz continuous in θ with constant $L' \leq L^*$. Let $\rho = \max\{|1 - \eta\mu^*|, |1 - \eta L^*|\}$. By the gradient descent convergence theorem, for learning rate, $\eta \in (0, 2/L^*)$, it follows that:

$$\lim_{t \rightarrow \infty} \|\theta^t - \theta^*\| \leq \lim_{t \rightarrow \infty} \rho^t \|\theta^0 - \theta^*\| = \|\theta^0 - \theta^*\| \lim_{t \rightarrow \infty} \rho^t = 0. \quad (18)$$

Therefore, $\lim_{t \rightarrow \infty} \theta^t = \theta^*$. Let $\beta^{t-1} = \mathcal{L}(\theta^{t-1}) / [\mathbf{1}_k^T \mathcal{L}(\theta^{t-1})]$, wherein $\beta^{t-1} \in [0, 1]^k$. Unrolling the recurrence relation from Eq. (5) and expressing it in terms of β^{t-1} , we obtain:

$$\alpha^t = (1 - \gamma)^t \alpha^0 + \gamma \sum_{l=0}^{t-1} (1 - \gamma)^{t-1-l} \beta^l. \quad (19)$$

Taking the limit and re-indexing the summation using $n = t - 1 - l$ and $l = t - 1 - n$, we obtain:

$$\lim_{t \rightarrow \infty} \alpha^t = \lim_{t \rightarrow \infty} \left[(1 - \gamma)^t \alpha^0 \right] + \lim_{t \rightarrow \infty} \left[\gamma \sum_{n=0}^{t-1} (1 - \gamma)^n \beta^{t-1-n} \right] \quad (20)$$

$$= \mathbf{0}_k + \gamma \lim_{t \rightarrow \infty} \left[\sum_{n=0}^{t-1} (1 - \gamma)^n \beta^{t-1-n} \right]. \quad (21)$$

We proceed with the steps to invoke the dominated convergence theorem. We note that for fixed n :

$$\lim_{t \rightarrow \infty} \left[(1 - \gamma)^n \beta^{t-1-n} \right] = (1 - \gamma)^n \lim_{t \rightarrow \infty} \left[\frac{\mathcal{L}(\theta^{t-1})}{\mathbf{1}_k^T \mathcal{L}(\theta^{t-1})} \right] = (1 - \gamma)^n \frac{\mathcal{L}(\theta^*)}{\mathbf{1}_k^T \mathcal{L}(\theta^*)}. \quad (22)$$

Now, consider $g(n) = (1 - \gamma)^n$. For this choice of $g(n)$, we have that:

$$\| (1 - \gamma)^n \beta^{t-1-n} \| \leq (1 - \gamma)^n \| \beta^{t-1-n} \| \leq g(n), \quad \forall t, n \in \mathbb{N} \quad (23)$$

$$\sum_{n=0}^{\infty} g(n) = \sum_{n=0}^{\infty} (1 - \gamma)^n = \frac{1}{1 - (1 - \gamma)} = \frac{1}{\gamma} < \infty. \quad (24)$$

We now invoke the dominated convergence theorem. Recalling Eq. (21), we observe that:

$$\lim_{t \rightarrow \infty} \alpha^t = \gamma \lim_{t \rightarrow \infty} \left[\sum_{n=0}^{t-1} (1 - \gamma)^n \beta^{t-1-n} \right] \quad (25)$$

$$= \gamma \sum_{n=0}^{\infty} (1 - \gamma)^n \lim_{t \rightarrow \infty} \beta^{t-1-n} = \gamma \sum_{n=0}^{\infty} (1 - \gamma)^n \frac{\mathcal{L}(\theta^*)}{\mathbf{1}_k^T \mathcal{L}(\theta^*)} \quad (26)$$

$$= (\gamma) \left(\frac{1}{\gamma} \right) \frac{\mathcal{L}(\theta^*)}{\mathbf{1}_k^T \mathcal{L}(\theta^*)} = \frac{\mathcal{L}(\theta^*)}{\mathbf{1}_k^T \mathcal{L}(\theta^*)} = \alpha^*. \quad (27)$$

Therefore, $\lim_{t \rightarrow \infty} \alpha^t = \alpha^* = \mathcal{L}(\theta^*) / [\mathbf{1}_k^T \mathcal{L}(\theta^*)]$. Cumulatively, for $\eta \in (0, 2/L^*)$ and $\gamma \in (0, 1)$, under learn2mix training, $\lim_{t \rightarrow \infty} \theta^t = \theta^*$, and $\lim_{t \rightarrow \infty} \alpha^t = \alpha^* = \mathcal{L}(\theta^*) / [\mathbf{1}_k^T \mathcal{L}(\theta^*)]$. \square

Corollary 2.4. Let $\mathcal{L}(\theta^t) \in \mathbb{R}^k$ denote the class-wise loss vector at time t . Suppose each class-wise loss, $\mathcal{L}_i(\theta) \in \mathbb{R}$, is strongly convex in θ , with strong convexity parameter $\mu_i \in \mathbb{R}_{>0}$, $\forall i \in \{1, \dots, k\}$, and suppose each class-wise loss gradient $\nabla_{\theta} \mathcal{L}_i(\theta) \in \mathbb{R}^m$ is Lipschitz continuous in θ with Lipschitz constant $L_i \in \mathbb{R}_{\geq 0}$, $\forall i \in \{1, \dots, k\}$. Let $\mu^* = \min_{i \in \{1, \dots, k\}} \mu_i$, $L^* = \max_{i \in \{1, \dots, k\}} L_i$. Then, the following holds, $\forall \alpha \in [0, 1]^k$, with $\sum_{i=1}^k \alpha_i = 1$:

$$\frac{\mu^*}{2} \|\theta^t - \theta^*\| \leq \|\nabla_{\theta} \mathcal{L}(\theta^t, \alpha)\| \leq L^* \|\theta^t - \theta^*\|, \quad (28)$$

$$\text{Wherein: } \|\nabla_{\theta} \mathcal{L}(\theta^t, \alpha^t)\| + \|\nabla_{\theta} \mathcal{L}(\theta^t, \tilde{\alpha})\| \leq 2L^* \|\theta^t - \theta^*\|. \quad (29)$$

Proof. We begin by recalling that $\mathcal{L}_i(\theta)$ is strongly convex in θ with strong convexity parameter μ_i , $\forall i \in \{1, \dots, k\}$. Accordingly, $\forall \alpha \in [0, 1]^k$, with $\sum_{i=1}^k \alpha_i = 1$, the loss function $\mathcal{L}(\theta, \alpha)$ is strongly convex in θ with parameter, $\mu' \in \mathbb{R}_{>0}$, which is lower bounded by $\mu^* \in \mathbb{R}_{>0}$, as per Eq. (30).

$$\mu' \geq \mu^* > 0, \quad \text{where: } \mu^* = \min_{i \in \{1, \dots, k\}} \mu_i, \quad \text{and: } \mu' = \sum_{i=1}^k \alpha_i \mu_i. \quad (30)$$

Now, recall that $\nabla_{\theta} \mathcal{L}_i(\theta)$, is Lipschitz continuous in θ with Lipschitz constant L_i , $\forall i \in \{1, \dots, k\}$. Accordingly, $\forall \alpha \in [0, 1]^k$, where $\sum_{i=1}^k \alpha_i = 1$, the loss gradient $\nabla_{\theta} \mathcal{L}(\theta, \alpha)$ is Lipschitz continuous in θ with Lipschitz constant, $L' \in \mathbb{R}_{\geq 0}$, which is upper bounded by $L^* \in \mathbb{R}_{\geq 0}$, as per Eq. (31).

$$L^* \geq L' \geq 0, \quad \text{where: } L^* = \max_{i \in \{1, \dots, k\}} L_i, \quad \text{and: } L' = \sum_{i=1}^k \alpha_i L_i. \quad (31)$$

Note that $\nabla_{\theta}\mathcal{L}(\theta^*, \alpha) = \mathbf{0}_m$. Since $\mathcal{L}(\theta, \alpha)$ is strongly convex in θ , the following inequalities hold:

$$\mathcal{L}(\theta^t, \alpha) - \mathcal{L}(\theta^*, \alpha) \geq \nabla_{\theta}\mathcal{L}(\theta^*, \alpha)^T(\theta^t - \theta^*) + \frac{\mu'}{2}\|\theta^t - \theta^*\|^2 = \frac{\mu'}{2}\|\theta^t - \theta^*\|^2, \quad (32)$$

$$\mathcal{L}(\theta^t, \alpha) - \mathcal{L}(\theta^*, \alpha) \leq \nabla_{\theta}\mathcal{L}(\theta^t, \alpha)^T(\theta^t - \theta^*) \leq \|\nabla_{\theta}\mathcal{L}(\theta^t, \alpha)\|\|\theta^t - \theta^*\|. \quad (33)$$

Combining Eq. (32) and Eq. (33), and recalling Eq. (30), we obtain the following inequality:

$$\|\nabla_{\theta}\mathcal{L}(\theta^t, \alpha)\| \geq \frac{\mathcal{L}(\theta^t, \alpha) - \mathcal{L}(\theta^*, \alpha)}{\|\theta^t - \theta^*\|} \geq \frac{\mu^*}{2}\|\theta^t - \theta^*\|. \quad (34)$$

Furthermore, since $\nabla_{\theta}\mathcal{L}(\theta, \alpha)$ is Lipschitz continuous in θ and recalling Eq. (31), it follows that:

$$\|\nabla_{\theta}\mathcal{L}(\theta^t, \alpha) - \nabla_{\theta}\mathcal{L}(\theta^*, \alpha)\| \leq L'\|\theta^t - \theta^*\| \implies \|\nabla_{\theta}\mathcal{L}(\theta^t, \alpha)\| \leq L^*\|\theta^t - \theta^*\|. \quad (35)$$

Altogether, combining Eq. (34) and Eq. (35), we arrive at the final inequality:

$$\frac{\mu^*}{2}\|\theta^t - \theta^*\| \leq \|\nabla_{\theta}\mathcal{L}(\theta^t, \alpha)\| \leq L^*\|\theta^t - \theta^*\|. \quad (36)$$

Furthermore, since Eq. (35) holds $\forall \alpha \in [0, 1]^k$ where $\sum_{i=1}^k \alpha_i = 1$, it follows that:

$$\|\nabla_{\theta}\mathcal{L}(\theta^t, \alpha^t)\| + \|\nabla_{\theta}\mathcal{L}(\theta^t, \tilde{\alpha})\| \leq 2L^*\|\theta^t - \theta^*\|. \quad (37)$$

□

Proposition 2.5. Let $\mathcal{L}(\theta^t), \mathcal{L}(\theta^*) \in \mathbb{R}^k$ denote the respective class-wise loss vectors for the model parameters at time t and for the optimal model parameters. Suppose each class-wise loss, $\mathcal{L}_i(\theta) \in \mathbb{R}$ is strongly convex in θ with strong convexity parameter $\mu_i \in \mathbb{R}_{>0}$, $\forall i \in \{1, \dots, k\}$, and each class-wise loss gradient $\nabla_{\theta}\mathcal{L}_i(\theta) \in \mathbb{R}^m$ is Lipschitz continuous in θ , having Lipschitz constant $L_i \in \mathbb{R}_{\geq 0}$, $\forall i \in \{1, \dots, k\}$. Moreover, suppose that the loss gradient $\nabla_{\theta}\mathcal{L}(\theta, \alpha) \in \mathbb{R}^m$ is Lipschitz continuous in α , having Lipschitz constant $L_{\alpha} \in \mathbb{R}_{\geq 0}$, and let $\mu^* = \min_{i \in \{1, \dots, k\}} \mu_i$, $L^* = \max_{i \in \{1, \dots, k\}} L_i$. Then, if and only if the following holds:

$$\left[\left(\frac{\mu^*}{2} - L^* \right) \|\theta^t - \theta^*\|^2 + \tilde{\alpha}^T (\mathcal{L}(\theta^t) - \mathcal{L}(\theta^*)) \right] \left[\|\theta^t - \theta^*\| - (\mathcal{L}(\theta^t) - \mathcal{L}(\theta^*)) \right] > 0, \quad (38)$$

It follows that for every learning rate, $\eta > 0$, and for every mixing rate, $\gamma \in (0, \beta]$:

$$\|(\theta^t - \eta\nabla_{\theta}\mathcal{L}(\theta^t, \alpha^t)) - \theta^*\| \leq \|(\theta^t - \eta\nabla_{\theta}\mathcal{L}(\theta^t, \tilde{\alpha})) - \theta^*\|, \quad (39)$$

$$\text{Where: } \beta = \frac{\left(\frac{\mu^*}{2} - L^* \right) \|\theta^t - \theta^*\|^2 + \tilde{\alpha}^T (\mathcal{L}(\theta^t) - \mathcal{L}(\theta^*))}{\eta L_{\alpha} L^* \left\| \frac{\mathcal{L}(\theta^{t-1})}{\mathbf{1}_k^T \mathcal{L}(\theta^{t-1})} - \tilde{\alpha} \right\| \left[\|\theta^t - \theta^*\| - (\mathcal{L}(\theta^t) - \mathcal{L}(\theta^*)) \right]} \quad (40)$$

Proof. We note that for all subsequent derivations, $\mathcal{F}(\theta^t, \theta^*, \eta, \alpha^t) = \|(\theta^t - \eta\nabla_{\theta}\mathcal{L}(\theta^t, \alpha^t)) - \theta^*\|$, and $\mathcal{G}(\theta^t, \theta^*, \eta, \tilde{\alpha}) = \|(\theta^t - \eta\nabla_{\theta}\mathcal{L}(\theta^t, \tilde{\alpha})) - \theta^*\|$, where $\alpha^{t-1} = \tilde{\alpha}$. We begin by observing that:

$$[\mathcal{F}(\theta^t, \theta^*, \eta, \alpha^t)]^2 = \|\theta^t - \theta^*\|^2 - 2\eta(\theta^t - \theta^*)^T \nabla_{\theta}\mathcal{L}(\theta^t, \alpha^t) + \eta^2 \|\nabla_{\theta}\mathcal{L}(\theta^t, \alpha^t)\|^2, \quad (41)$$

$$[\mathcal{G}(\theta^t, \theta^*, \eta, \tilde{\alpha})]^2 = \|\theta^t - \theta^*\|^2 - 2\eta(\theta^t - \theta^*)^T \nabla_{\theta}\mathcal{L}(\theta^t, \tilde{\alpha}) + \eta^2 \|\nabla_{\theta}\mathcal{L}(\theta^t, \tilde{\alpha})\|^2. \quad (42)$$

Accordingly, the difference between $[\mathcal{F}(\theta^t, \theta^*, \eta, \alpha^t)]^2$ and $[\mathcal{G}(\theta^t, \theta^*, \eta, \tilde{\alpha})]^2$ is given by:

$$\begin{aligned} [\mathcal{F}(\theta^t, \theta^*, \eta, \alpha^t)]^2 - [\mathcal{G}(\theta^t, \theta^*, \eta, \tilde{\alpha})]^2 &= -2\eta[(\theta^t - \theta^*)^T (\nabla_{\theta}\mathcal{L}(\theta^t, \alpha^t) - \nabla_{\theta}\mathcal{L}(\theta^t, \tilde{\alpha}))] \\ &\quad + \eta^2 [\|\nabla_{\theta}\mathcal{L}(\theta^t, \alpha^t)\|^2 - \|\nabla_{\theta}\mathcal{L}(\theta^t, \tilde{\alpha})\|^2]. \end{aligned} \quad (43)$$

Consequently, suppose that $\mathcal{H}(\theta^t, \theta^*, \eta, \tilde{\alpha}, \alpha^t) = 2\eta[(\theta^t - \theta^*)^T (\nabla_{\theta}\mathcal{L}(\theta^t, \alpha^t) - \nabla_{\theta}\mathcal{L}(\theta^t, \tilde{\alpha}))]$, and let $\mathcal{J}(\theta^t, \eta, \tilde{\alpha}, \alpha^t) = \eta^2 [\|\nabla_{\theta}\mathcal{L}(\theta^t, \alpha^t)\|^2 - \|\nabla_{\theta}\mathcal{L}(\theta^t, \tilde{\alpha})\|^2]$. Suppose the loss gradient, $\nabla_{\theta}\mathcal{L}(\theta, \alpha)$, is Lipschitz continuous in α with Lipschitz

constant, L_α . We now upper bound $\mathcal{J}(\theta^t, \eta, \tilde{\alpha}, \alpha^t)$:

$$\begin{aligned} \mathcal{J}(\theta^t, \eta, \alpha, \alpha^t) &= \eta^2 [\nabla_\theta \mathcal{L}(\theta^t, \alpha^t) - \nabla_\theta \mathcal{L}(\theta^t, \tilde{\alpha})]^T [\nabla_\theta \mathcal{L}(\theta^t, \alpha^t) + \nabla_\theta \mathcal{L}(\theta^t, \tilde{\alpha})] \\ &\leq \|\nabla_\theta \mathcal{L}(\theta^t, \alpha^t) - \nabla_\theta \mathcal{L}(\theta^t, \tilde{\alpha})\| \|\nabla_\theta \mathcal{L}(\theta^t, \alpha^t) + \nabla_\theta \mathcal{L}(\theta^t, \tilde{\alpha})\| \end{aligned} \quad (44)$$

$$\leq 2\eta^2 L_\alpha \|\alpha^t - \tilde{\alpha}\| \left[\|\nabla_\theta \mathcal{L}(\theta^t, \alpha^t)\| + \|\nabla_\theta \mathcal{L}(\theta^t, \tilde{\alpha})\| \right] \quad (45)$$

$$\leq 2\eta^2 L_\alpha L^* \|\alpha^t - \tilde{\alpha}\| \|\theta^t - \theta^*\| \quad (46)$$

$$= 2\eta^2 L_\alpha L^* \left\| \tilde{\alpha} + \gamma \left(\frac{\mathcal{L}(\theta^{t-1})}{\mathbf{1}_k^T \mathcal{L}(\theta^{t-1})} - \tilde{\alpha} \right) - \tilde{\alpha} \right\| \|\theta^t - \theta^*\| \quad (47)$$

$$= 2\eta^2 L_\alpha L^* \gamma \left\| \frac{\mathcal{L}(\theta^{t-1})}{\mathbf{1}_k^T \mathcal{L}(\theta^{t-1})} - \tilde{\alpha} \right\| \|\theta^t - \theta^*\|. \quad (48)$$

We note that this upper bound follows from the Cauchy-Schwarz inequality and Corollary 2.4. We now proceed by lower bounding $\mathcal{H}(\theta^t, \theta^*, \eta, \tilde{\alpha}, \alpha^t)$:

$$\mathcal{H}(\theta^t, \theta^*, \eta, \tilde{\alpha}, \alpha^t) = 2\eta \left[(\theta^t - \theta^*)^T \nabla_\theta \mathcal{L}(\theta^t, \alpha^t) - (\theta^t - \theta^*)^T \nabla_\theta \mathcal{L}(\theta^t, \tilde{\alpha}) \right] \quad (49)$$

$$\geq 2\eta \left[(\theta^t - \theta^*)^T \nabla_\theta \mathcal{L}(\theta^t, \alpha^t) - \|\theta^t - \theta^*\| \|\nabla_\theta \mathcal{L}(\theta^t, \tilde{\alpha})\| \right] \quad (50)$$

$$\geq 2\eta \left[(\theta^t - \theta^*)^T \nabla_\theta \mathcal{L}(\theta^t, \alpha^t) - L^* \|\theta^t - \theta^*\|^2 \right] \quad (51)$$

$$= 2\eta \left[\frac{\mu^*}{2} \|\theta^t - \theta^*\|^2 + \mathcal{L}(\theta^t, \alpha^t) - \mathcal{L}(\theta^*, \alpha^t) - L^* \|\theta^t - \theta^*\|^2 \right] \quad (52)$$

$$\begin{aligned} &= 2\eta \left[\left(\frac{\mu^*}{2} - L^* \right) \|\theta^t - \theta^*\|^2 + \tilde{\alpha}^T (\mathcal{L}(\theta^t) - \mathcal{L}(\theta^*)) \right. \\ &\quad \left. + \gamma \left(\frac{\mathcal{L}(\theta^{t-1})}{\mathbf{1}_k^T \mathcal{L}(\theta^{t-1})} - \tilde{\alpha} \right)^T (\mathcal{L}(\theta^t) - \mathcal{L}(\theta^*)) \right]. \end{aligned} \quad (53)$$

As in above, we note that this lower bound also follows from the Cauchy-Schwarz inequality and Corollary 2.4, and further invokes the strong convexity of $\mathcal{L}(\theta, \alpha)$ in θ . Combining Eq. (48) and Eq. (53), we obtain the following upper bound on $[\mathcal{F}(\theta^t, \theta^*, \eta, \alpha^t)]^2 - [\mathcal{G}(\theta^t, \theta^*, \eta, \tilde{\alpha})]^2$:

$$[\mathcal{F}(\theta^t, \theta^*, \eta, \alpha^t)]^2 - [\mathcal{G}(\theta^t, \theta^*, \eta, \tilde{\alpha})]^2 \leq \mathcal{K}(\theta^t, \theta^*, \eta, \gamma, \tilde{\alpha}, \alpha^t), \quad (54)$$

$$\begin{aligned} \text{Where: } \mathcal{K}(\theta^t, \theta^*, \eta, \gamma, \tilde{\alpha}, \alpha^t) &= -2\eta \left[\left(\frac{\mu^*}{2} - L^* \right) \|\theta^t - \theta^*\|^2 + \tilde{\alpha}^T (\mathcal{L}(\theta^t) - \mathcal{L}(\theta^*)) \right. \\ &\quad \left. + \gamma \left(\frac{\mathcal{L}(\theta^{t-1})}{\mathbf{1}_k^T \mathcal{L}(\theta^{t-1})} - \tilde{\alpha} \right)^T (\mathcal{L}(\theta^t) - \mathcal{L}(\theta^*)) \right] \\ &\quad + 2\eta^2 L_\alpha L^* \gamma \left\| \frac{\mathcal{L}(\theta^{t-1})}{\mathbf{1}_k^T \mathcal{L}(\theta^{t-1})} - \tilde{\alpha} \right\| \|\theta^t - \theta^*\|. \end{aligned} \quad (55)$$

Now, consider the following chain of inequalities deriving from Eq. (54):

$$\begin{aligned} \mathcal{K}(\theta^t, \theta^*, \eta, \gamma, \tilde{\alpha}, \alpha^t) \leq 0 &\implies [\mathcal{F}(\theta^t, \theta^*, \eta, \alpha^t)]^2 - [\mathcal{G}(\theta^t, \theta^*, \eta, \tilde{\alpha})]^2 \leq 0 \\ &\implies [\mathcal{F}(\theta^t, \theta^*, \eta, \alpha^t)] \leq [\mathcal{G}(\theta^t, \theta^*, \eta, \tilde{\alpha})]. \end{aligned} \quad (56)$$

Accordingly, we aim to find a condition on the mixing rate, γ , under which the chain of inequalities is satisfied. We proceed by letting $\mathcal{K}(\theta^t, \theta^*, \eta, \gamma, \tilde{\alpha}, \alpha^t) \leq 0$, and rearrange the terms:

$$\begin{aligned} \left(\frac{\mu^*}{2} - L^* \right) \|\theta^t - \theta^*\|^2 + \tilde{\alpha}^T (\mathcal{L}(\theta^t) - \mathcal{L}(\theta^*)) &\geq \gamma \left[\eta L_\alpha L^* \left\| \frac{\mathcal{L}(\theta^{t-1})}{\mathbf{1}_k^T \mathcal{L}(\theta^{t-1})} - \tilde{\alpha} \right\| \|\theta^t - \theta^*\| \right. \\ &\quad \left. - \left(\frac{\mathcal{L}(\theta^{t-1})}{\mathbf{1}_k^T \mathcal{L}(\theta^{t-1})} - \tilde{\alpha} \right)^T (\mathcal{L}(\theta^t) - \mathcal{L}(\theta^*)) \right]. \end{aligned} \quad (57)$$

We note that this chain of inequalities is satisfied if, for every $\eta > 0$:

$$0 < \gamma \leq \frac{\left(\frac{\mu^*}{2} - L^*\right) \|\theta^t - \theta^*\|^2 + \tilde{\alpha}^T (\mathcal{L}(\theta^t) - \mathcal{L}(\theta^*))}{\eta L_\alpha L^* \left\| \frac{\mathcal{L}(\theta^{t-1})}{\mathbb{1}_k^T \mathcal{L}(\theta^{t-1})} - \tilde{\alpha} \right\| \|\theta^t - \theta^*\| - \left(\frac{\mathcal{L}(\theta^{t-1})}{\mathbb{1}_k^T \mathcal{L}(\theta^{t-1})} - \tilde{\alpha} \right)^T (\mathcal{L}(\theta^t) - \mathcal{L}(\theta^*))} \leq \beta, \quad (58)$$

$$\text{Where: } \beta = \frac{\left(\frac{\mu^*}{2} - L^*\right) \|\theta^t - \theta^*\|^2 + \tilde{\alpha}^T (\mathcal{L}(\theta^t) - \mathcal{L}(\theta^*))}{\eta L_\alpha L^* \left\| \frac{\mathcal{L}(\theta^{t-1})}{\mathbb{1}_k^T \mathcal{L}(\theta^{t-1})} - \tilde{\alpha} \right\| \left[\|\theta^t - \theta^*\| - (\mathcal{L}(\theta^t) - \mathcal{L}(\theta^*)) \right]}. \quad (59)$$

However, $\gamma > 0$ iff the numerator and denominator from Eq. (59) have the same sign, ensuring that $\beta > 0$. Accordingly, if and only if the condition provided in Eq. (60) is satisfied:

$$\left[\left(\frac{\mu^*}{2} - L^* \right) \|\theta^t - \theta^*\|^2 + \tilde{\alpha}^T (\mathcal{L}(\theta^t) - \mathcal{L}(\theta^*)) \right] \left[\|\theta^t - \theta^*\| - (\mathcal{L}(\theta^t) - \mathcal{L}(\theta^*)) \right] > 0, \quad (60)$$

It follows that for every learning rate $\eta > 0$, and for every mixing rate $\gamma \in (0, \beta]$ satisfying Eq. (59):

$$\|(\theta^t - \eta \nabla_\theta \mathcal{L}(\theta^t, \alpha^t)) - \theta^*\| \leq \|(\theta^t - \eta \nabla_\theta \mathcal{L}(\theta^t, \tilde{\alpha})) - \theta^*\|. \quad (61)$$

□

B DATASET DESCRIPTIONS

B.1 MNIST DATASET

The **MNIST** (Modified National Institute of Standards and Technology) dataset is a collection of handwritten digits commonly used to train image processing systems. For the MNIST classification result from Section 4.1, the original training dataset, J , comprises $N = 60000$ samples, wherein the fixed-proportion mixing parameters (for default numerical class ordering of digits from 1 – 10) are:

$$\tilde{\alpha} = [0.0987, 0.1124, 0.0993, 0.1022, 0.0974, 0.0904, 0.0986, 0.1044, 0.0975, 0.0991]^T$$

The test dataset, K , comprises $N_{\text{test}} = 10000$ samples, with class proportions equivalent to the class proportions in the base MNIST test dataset. For MNIST reconstruction (see Section 4.3), we utilize manual class imbalancing, reducing the number of samples comprising each numerical class 6 – 10 by a factor of 5. The original training dataset, J , now contains $N = 36475$ samples, wherein the fixed-proportion mixing parameters (for default numerical class ordering of digits from 1 – 10) are:

$$\tilde{\alpha} = [0.1624, 0.1848, 0.1633, 0.1681, 0.1602, 0.0297, 0.0324, 0.0344, 0.0321, 0.0326]^T$$

We note that the test dataset maintains the same class proportions as in the base MNIST test dataset. The features and labels within MNIST are summarized as follows:

- Each feature (image) is of size 28×28 , representing grayscale intensities from 0 to 255.
- Target Variable: The numerical class (digit) the image represents, ranging from 1 to 10.

B.2 FASHION MNIST DATASET

The **Fashion MNIST** dataset is a collection of clothing images commonly used to train image processing systems. For the Fashion MNIST classification result from Section 4.1, the original training dataset, J , consists of $N = 60000$ samples, wherein the fixed-proportion mixing parameters (for default numerical class ordering of clothing from 1 – 10) are:

$$\tilde{\alpha} = [0.1, 0.1, 0.1, 0.1, 0.1, 0.1, 0.1, 0.1, 0.1, 0.1]^T = (0.1) \mathbb{1}_{10}$$

The test dataset, K , comprises $N_{\text{test}} = 10000$ samples, with class proportions equivalent to the class proportions in the base Fashion MNIST test dataset. For Fashion MNIST reconstruction (see Section 4.3), we use manual class imbalancing, reducing the number of samples within each numerical class 6 – 10 by a factor of 5. The original training dataset J , now

has $N = 36000$ samples. The fixed-proportion mixing parameters (for default numerical class ordering of clothing from 1 – 10) are:

$$\tilde{\alpha} = [(0.1667)\mathbf{1}_5^T, (0.0333)\mathbf{1}_5^T]^T$$

We note that the test dataset maintains the same class proportions as in the base Fashion MNIST test dataset. The features and labels within Fashion MNIST are summarized as follows:

- Each feature (image) is of size 28×28 , representing grayscale intensities from 0 to 255.
- Target Variable: The numerical class (clothing) the image represents, ranging from 1 to 10.

B.3 CIFAR-10 DATASET

The **CIFAR-10** dataset is a collection of color images categorized into 10 different classes, and is commonly used to train image processing systems. For the CIFAR-10 classification result in Section 4.1, the original training dataset, J , comprises $N = 50000$ samples, wherein the fixed-proportion mixing parameters (for default numerical class ordering of categories from 1 – 10) are:

$$\tilde{\alpha} = (0.1)\mathbf{1}_{10}$$

The test dataset, K , comprises $N_{\text{test}} = 10000$ samples, with class proportions equivalent to the class proportions in the base CIFAR-10 test dataset. For CIFAR-10 reconstruction (see Section 4.3), we use manual class imbalancing, reducing the number of samples in numerical classes 1 – 4, 7 – 10 by a factor of 10. The original training dataset, J , now has $N = 14000$ samples. The fixed-proportion mixing parameters (for default numerical class ordering of categories from 1 – 10) are:

$$\tilde{\alpha} = [(0.0357)\mathbf{1}_4^T, (0.3571)\mathbf{1}_2^T, (0.0357)\mathbf{1}_4^T]^T$$

We note that the test dataset maintains the same class proportions found in the base CIFAR-10 test dataset. The features and labels within CIFAR-10 are summarized as follows:

- Each feature (image) is of size $32 \times 32 \times 3$, with three color channels (RGB), and size 32 x 32 pixels for each channel, represented as a grayscale intensity from 0 to 255.
- Target Variable: The numerical class (category) the image represents, ranging from 1 to 10.

B.4 IMAGENETTE DATASET

The **Imagenette** dataset contains a subset of 10 classes from the ImageNet dataset of color images, and is commonly used to train image processing systems. The base Imagenette training dataset, I , comprises $N_I = 9469$ samples, and the base Imagenette test dataset, K , comprises $N_{\text{test}} = 3925$ samples. For the Imagenette classification result in Section 4.1, we utilize manual class imbalancing. Let $N_i \in \mathbb{N}$ be the number of samples in each class, $i \in \{1, \dots, 10\}$, from I , where $N_I = \sum_{i=1}^{10} N_i$. We define $\epsilon_i = 1 - 0.1i, \forall i \in \{1, \dots, 10\}$ as the linearly decreasing *imbalance factor*. Accordingly, the original training dataset, J , has $N = \sum_{i=1}^{10} \epsilon_i N_i = 5207$ samples. The fixed-proportion mixing parameters (for default numerical class ordering of categories from 1 – 10) are:

$$\tilde{\alpha} = [0.1849, 0.1650, 0.1525, 0.1152, 0.1083, 0.0918, 0.0737, 0.0536, 0.0365, 0.0184]^T$$

We note that the test dataset maintains the same class proportions found in the base Imagenette test dataset. The features and labels within Imagenette are summarized as follows:

- Each feature (image) is of size $224 \times 224 \times 3$, with three color channels (RGB), and size 224 x 224 pixels for each channel, represented as a grayscale intensity from 0 to 255.
- Target Variable: The numerical class (category) the image represents, ranging from 1 to 10.

B.5 CIFAR-100 DATASET

The **CIFAR-100** dataset is a collection of color images categorized into 100 different classes, and is commonly used to train image processing systems. The base CIFAR-100 training dataset, I , has $N_I = 50000$ samples, and the base CIFAR-100 test dataset, K , has $N_{\text{test}} = 10000$ samples. For the CIFAR-100 classification result in Section 4.1, we utilize manual class

imbalancing. Let $N_i \in \mathbb{N}$ be the number of samples in each class, $i \in \{1, \dots, 100\}$, from I , whereby $N_I = \sum_{i=1}^{100} N_i$. We define $\epsilon_i = 40^{-i/100}$, $\forall i \in \{1, \dots, 100\}$ as the logarithmically decreasing *imbalance factor*. Accordingly, the original training dataset, J , has $N = \sum_{i=1}^{100} \epsilon_i N_i = 13209$ samples. The fixed-proportion mixing parameters (for default numerical class ordering of categories from 1 – 100) are:

$$\tilde{\alpha} = [\tilde{\alpha}_1, \tilde{\alpha}_2, \dots, \tilde{\alpha}_{100}]^T, \quad \text{where: } \tilde{\alpha}_i = (\epsilon_i N_i) / N, \quad \forall i \in \{1, \dots, 100\}$$

We note that the test dataset maintains the same class proportions found in the base CIFAR-100 test dataset. The features and labels within CIFAR-100 are summarized as follows:

- Each feature (image) is of size $32 \times 32 \times 3$, with three color channels (RGB), and size 32 x 32 pixels for each channel, represented as a grayscale intensity from 0 to 255.
- Target Variable: The numerical class (category) the image denotes, ranging from 1 to 100.

B.6 IMDB DATASET

The **IMDB** dataset is a collection of movie reviews, categorized as positive or negative in sentiment. We split the IMDB dataset such that the base IMDB training dataset, I , has $N_I = 40000$ samples, and the base IMDB test dataset, K , consists of $N_{\text{test}} = 10000$ samples. For the IMDB classification result in Section 4.1, we leverage manual class imbalancing, wherein numerical class 1 retains 30% of its samples. Accordingly, the original training dataset, J , has $N = 26000$ samples. The fixed-proportion mixing parameters (for default numerical class ordering of sentiment from 1, 2) are:

$$\tilde{\alpha} = [0.2307, 0.7693]^T$$

We note that the test dataset maintains the same class proportions as in the base IMDB test dataset. The features and labels within the IMDB dataset are summarized as follows:

- Each feature (review) is tokenized and encoded as a sequence of word indices with a max length of 500 tokens. Sequences are padded or truncated to ensure uniform length.
- Target Variable: The numerical class (sentiment) the review represents, either 1 or 2.

B.7 MEAN ESTIMATION DATASET

The **Mean Estimation** dataset is a synthetic benchmark designed for regression tasks, wherein each example, (x_j, y_j) , comprises a 10-dimensional feature vector, x_j , of samples from one of four statistical distributions, and the mean, y_j , of this distribution. We create an imbalanced original training dataset, J , with $N = 3000$ samples, where J_1 has 1000 examples drawn from a normal distribution with $\sigma = 1$, J_2 has 1000 examples drawn from an exponential distribution, J_3 has 800 examples drawn from a chi-squared distribution, and J_4 has 200 samples drawn from a uniform distribution. The fixed-proportion mixing parameters (for numerical ordering of distributions from 1 – 4) are:

$$\tilde{\alpha} = [0.333, 0.333, 0.267, 0.067]^T$$

The test dataset, K , is created as a balanced dataset that has 1000 examples from each distribution, wherein $N_{\text{test}} = 4000$. The Mean Estimation dataset features and labels are summarized as follows:

- Each feature (vector of samples) is generated from one of four statistical distributions (normal, exponential, chi-squared, uniform). The feature vectors are created by sampling from these distributions with means uniformly drawn from the interval $[0, 1]$ for normal, exponential, and chi-squared distributions, and from $[20, 50]$ for the uniform distribution.
- Target Variable: The mean parameter used to generate the vector of samples, representing the underlying expected value of the chosen distribution.

B.8 WINE QUALITY DATASET

The **Wine Quality** dataset consists of physicochemical tests on white and red wine samples, and the corresponding quality rating. We treat the wine type (white = 1, red = 2) as a categorical variable, wherein $k = 2$. We split the Wine Quality

dataset such that the base Wine Quality training dataset, J , has $N = 3248$ samples, and the base Wine Quality test dataset, K , has $N_{\text{test}} = 3249$ samples. For the Wine Quality regression result in Section 4.2, we utilize manual class imbalancing, reducing the number of samples in numerical class 1 by a factor of 10. The original training dataset, J , now has $N = 1043$ samples, where the fixed-proportion mixing parameters (for numerical class ordering of wine type from 1, 2) are:

$$\tilde{\alpha} = [0.234, 0.766]^T$$

We note that the test dataset maintains the same class proportions as in the base Wine Quality test dataset. The features and labels within the Wine Quality dataset are summarized as follows:

- Each feature (physicochemical tests) contains a set of test results, and is of size 11×1 .
- Target Variable: The wine quality rating given to the set of physicochemical tests.

B.9 CALIFORNIA HOUSING DATASET

The **California Housing** dataset contains housing data from California and their associated prices. As the ocean proximity variable is categorical ($<1H$ OCEAN = 1, INLAND = 2, NEAR BAY = 3, NEAR OCEAN = 4), we denote $k = 4$. We split the California Housing dataset such that the base California Housing training dataset, J , has $N = 10214$ samples, and the base California Housing test dataset, K , has $N_{\text{test}} = 10214$ samples. For the California Housing regression result in Section 4.2, we use manual class imbalancing, reducing the number of samples in numerical classes 1, 2, 4 by a factor of 20. The original training dataset, J , now has $N = 3641$ samples. The fixed-proportion mixing parameters (for numerical class ordering of ocean proximity from 1 – 4) are:

$$\tilde{\alpha} = [0.0615, 0.9055, 0.0154, 0.0176]^T$$

We note that the test dataset maintains the same class proportions as in the base California Housing test dataset. The features and labels in the California Housing dataset are summarized as follows:

- Each feature (housing data) contains various housing attributes, and is of size 8×1 .
- Target Variable: The housing price associated with the housing data.

C EXPERIMENT DETAILS

C.1 NEURAL NETWORK ARCHITECTURES

We provide comprehensive descriptions for six different neural network architectures designed for various tasks: classification, regression, and image reconstruction. Each of these architectures were employed to generate the respective empirical results pertaining to the aforementioned tasks.

C.1.1 Fully Connected Networks

We leverage fully connected networks in our analysis for regression on Mean Estimation, California Housing, and Wine Quality. The network consists of the following layers, wherein $d = 10$ for Mean Estimation, $d = 11$ for Wine Quality, and $d = 8$ for California Housing:

- **Fully Connected Layer (`fc1`)**: Transforms the input features from a d -dimensional space to a 64-dimensional space.
- **ReLU Activation (`relu`)**: Applies the ReLU activation function to the output of `fc1`.
- **Fully Connected Layer (`fc2`)**: Maps the 64-dimensional representation from `relu` to a 1-dimensional output.

C.1.2 Convolutional Neural Networks

We utilize the LeNet-5 convolutional neural network architecture in our analysis for image classification on MNIST and Fashion MNIST. The network consists of the following layers:

- **Convolutional Layer (conv1)**: Applies a 2D convolution with 1 input channel, 6 output channels, and a kernel size of 5.
- **ReLU Activation (relu1)**: Applies the ReLU activation function to the output of conv1.
- **Max Pooling Layer (pool1)**: Performs 2x2 max pooling on the output of relu1.
- **Convolutional Layer (conv2)**: Applies a 2D convolution with 6 input channels, 16 output channels, and a kernel size of 5.
- **ReLU Activation (relu2)**: Applies the ReLU activation function to the output of conv2.
- **Max Pooling Layer (pool2)**: Performs 2x2 max pooling on the output of relu2.
- **Flatten Layer**: Reshapes the pooled feature maps into a 1D vector.
- **Fully Connected Layer (fc1)**: Maps the flattened vector to a 120-dimensional space.
- **ReLU Activation (relu3)**: Applies the ReLU activation function to the output of fc1.
- **Fully Connected Layer (fc2)**: Maps the 120-dimensional input to a 84-dimensional space.
- **ReLU Activation (relu4)**: Applies the ReLU activation function to the output of fc2.
- **Fully Connected Layer (fc3)**: Produces a 10-dimensional output for classification.

For image classification on CIFAR-10 and CIFAR-100, we employ an adapted, larger version of the LeNet-5 model. The network consists of the following layers, wherein $k = 10$ for CIFAR-10 and $k = 100$ for CIFAR-100.

- **Convolutional Layer (conv1)**: Applies 2D convolution with 3 input channels, 16 output channels, and a kernel size of 3.
- **ReLU Activation (relu1)**: Applies the ReLU activation function to the output of conv1.
- **Max Pooling Layer (pool1)**: Performs 2x2 max pooling on the output of relu1.
- **Convolutional Layer (conv2)**: Applies 2D convolution with 16 input channels, 32 output channels, and a kernel size of 3.
- **ReLU Activation (relu2)**: Applies the ReLU activation function to the output of conv2.
- **Max Pooling Layer (pool2)**: Performs 2x2 max pooling on the output of relu2.
- **Convolutional Layer (conv3)**: Applies 2D convolution with 32 input channels, 64 output channels, and a kernel size of 3.
- **ReLU Activation (relu3)**: Applies the ReLU activation function to the output of conv3.
- **Max Pooling Layer (pool3)**: Performs 2x2 max pooling on the output of relu3.
- **Flatten Layer**: Reshapes the pooled feature maps into a 1D vector of size $4 \times 4 \times 64$.
- **Fully Connected Layer (fc1)**: Maps the flattened vector to a 500-dimensional space.
- **ReLU Activation (relu4)**: Applies the ReLU activation function to the output of fc1.
- **Dropout Layer (dropout1)**: Applies dropout with $p = 0.5$ to the output of relu4.
- **Fully Connected Layer (fc2)**: Produces a k -dimensional output for classification.

C.1.3 Residual Neural Networks

For image classification on Imagenette, we employ the ResNet-18 residual neural network architecture, which consists of the following layers:

- **Convolutional Layer (conv1)**: Applies a 7x7 convolution with 3 input channels, 64 output channels, and a stride of 2.
- **Batch Normalization (bn1)**: Normalizes the output of conv1.
- **ReLU Activation (relu)**: Applies the ReLU activation function to the output of bn1.
- **Max Pooling Layer (maxpool1)**: Performs 3x3 max pooling with a stride of 2 on the output of relu.
- **Residual Layer 1 (layer1)**: Contains two residual blocks, each with 64 channels.

- **Residual Layer 2 (layer2)**: Contains two residual blocks, each with 128 channels.
- **Residual Layer 3 (layer3)**: Contains two residual blocks, each with 256 channels.
- **Residual Layer 4 (layer4)**: Contains two residual blocks, each with 512 channels.
- **Average Pooling (avgpool1)**: Applies adaptive average pooling to reduce the spatial dimensions to 1x1.
- **Fully Connected Layer (fc)**: Produces a 10-dimensional output for classification.

C.1.4 Transformer Models

For sentiment classification on IMDB Sentiment Analysis, we leverage a transformer architecture, which consists of the following layers:

- **Embedding Layer (embedding)**: Maps input tokens to 64-dimensional embeddings.
- **Positional Encoding (pos_encoder)**: Adds positional information to the embeddings with a maximum sequence length of 500.
- **Transformer Encoder (transformer_encoder)**: Applies a transformer encoder with 1 layer, 4 attention heads, and a hidden dimension of 128.
- **Pooling Layer (pool)**: Averages the transformer outputs across the sequence length.
- **Dropout Layer (dropout)**: Applies dropout with probability 0.1 to the pooled output.
- **Fully Connected Layer (fc1)**: Maps the 64-dimensional pooled vector to 32-dimensional space.
- **ReLU Activation (relu1)**: Applies the ReLU activation function to the output of fc1.
- **Fully Connected Layer (fc2)**: Maps the 32-dimensional input to 2 output classes.

C.1.5 Autoencoder Models

For image reconstruction on MNIST, Fashion MNIST, and CIFAR-10, we employ an autoencoder. This network consists of the following layers, where $d = 784$ for MNIST and Fashion MNIST, and $d = 3072$ for CIFAR-10:

- **Fully Connected Layer (fc1)**: Transforms the input features from a d -dimensional space to a 128-dimensional space.
- **ReLU Activation (relu1)**: Applies the ReLU activation function to the output of fc1.
- **Fully Connected Layer (fc2)**: Reduces the 128-dimensional representation to a 32-dimensional encoded vector.
- **Fully Connected Layer (fc3)**: Expands the 32-dimensional encoded vector back to a 128-dimensional space.
- **ReLU Activation (relu1)**: Applies the ReLU activation function to the output of fc3.
- **Fully Connected Layer (fc4)**: Maps the 128-dimensional representation back to the original d -dimensional space.
- **Sigmoid Activation (sigmoid1)**: Applies the Sigmoid activation function to ensure the output values are between 0 and 1.

C.2 FOCAL TRAINING

For the classification tasks outlined in Section 4.1, we compare learn2mix and classical training with focal loss-based neural network training (focal training). Let $\tilde{\alpha} \in [0, 1]^k$ denote the vector of fixed-proportion mixing parameters, let $\mathcal{L}(\theta^t) \in \mathbb{R}^k$ denote the vector of class-wise cross entropy losses at time t , and let $\omega \in \mathbb{R}^k$ denote the vector of class-wise weighting factors, where $\forall i \in \{1, \dots, k\}$:

$$\omega_i = \frac{[1/(\tilde{\alpha}_i N)]}{\sum_{i'=1}^k [1/(\tilde{\alpha}_{i'} N)]} \times k. \quad (62)$$

The vector of predicted class-wise probabilities, $p \in [0, 1]^k$, is given by $p = \exp(-\mathcal{L}(\theta^t))$, and we let $\Gamma \in \mathbb{R}_{\geq 0}$ be the focusing parameter. The focal loss at time t , $\mathcal{L}_{\text{FCL}}(\theta^t, \omega) \in \mathbb{R}_{\geq 0}$, is given by:

$$\mathcal{L}_{\text{FCL}}(\theta^t, \tilde{\alpha}) = \frac{1}{k} \sum_{i=1}^k (-\omega_i) (1 - p_i)^\Gamma \log(p_i). \quad (63)$$

Per the recommendations in [Lin et al., 2017], we choose $\Gamma = 2$ in compiling the empirical results.

C.3 SMOTE TRAINING

For the classification tasks outlined in Section 4.1, we also compare learn2mix and classical training with neural networks trained on SMOTE-oversampled datasets (SMOTE training). Let J denote the original training dataset, where the number of samples in each class, $i \in \{1, \dots, k\}$ is given by $\tilde{\alpha}_i N$. After applying SMOTE oversampling, we obtain a new training dataset, J^{SMOTE} , with uniform class proportions, $\tilde{\alpha}_i^{\text{SMOTE}} = \frac{1}{k}, \forall i \in \{1, \dots, k\}$. The total number of samples in J^{SMOTE} , is given by:

$$N^{\text{SMOTE}} = \left(\max_{i \in \{1, \dots, k\}} \tilde{\alpha}_i N \right) \times k. \quad (64)$$

In the original training dataset, J , we use a batch size of M , resulting in $P = N/M$ total batches. For consistency with learn2mix and classical training (see Section 4.1), we perform SMOTE training on P batches of size M from the SMOTE oversampled training dataset, J^{SMOTE} , during each epoch.

C.4 NEURAL NETWORK TRAINING HYPERPARAMETERS

The relevant hyperparameters used to train the neural networks outlined in Section C.1 are given in Table 3. All results presented in the main text were produced using these hyperparameter choices.

Table 3: Neural network training hyperparameters (grouped by task).

Dataset	Task	Optimizer	Learning Rate (η)	Mixing Rate (γ) (Learn2Mix)	Batch Size (M)
MNIST	Classification	Adam	1.0e-5	0.1	1000
Fashion MNIST	Classification	Adam	5.0e-6	0.5	1000
CIFAR-10	Classification	Adam	1.0e-5	0.1	1000
Imagenette	Classification	Adam	1.0e-6	0.1	100
CIFAR-100	Classification	Adam	0.0001	0.5	5000
IMDB	Classification	Adam	0.0001	0.1	500
Mean Estimation	Regression	Adam	5.0e-5	0.01	500
Wine Quality	Regression	Adam	0.0001	0.05	100
California Housing	Regression	Adam	5.0e-5	0.01	1000
MNIST	Reconstruction	Adam	0.0005	0.1	1000
Fashion MNIST	Reconstruction	Adam	1.0e-5	0.1	1000
CIFAR-10	Reconstruction	Adam	1.0e-5	0.1	1000